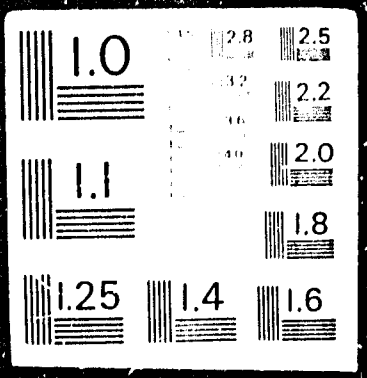

CARDE T.R. 595/68
PROJECT D46-95-51-10

UNCLASSIFIED

EXPERIMENTAL STUDY OF TURBULENT WAKES IN FREE-FLIGHT RANGES

D. Heckman*, L. Tardif*, C. Lahaye**

The content of this document was presented at the Symposium on Turbulence of Fluids and Plasma Sponsored by the Microwave Research Institute of the Polytechnic Institute of Brooklyn, 16-18 April 1968.

This research was sponsored jointly by

The Canadian Armament Research and Development Establishment
P.O. Box 1427,
Québec, P.Q. Canada.
Under Project D46-95-51-10
D46-99-10-35

The Advanced Research Projects Agency as part of Project DEFENDER ARPA Order 133
Monitored by the US Army Missile Command,
Redstone Arsenal, Alabama 35809
Contract DA-01-021-AMC-14468 (Z)

* Defence Scientific Service Officers
** Research Scientist, Computing Devices of Canada Ltd., attached to Aerophysics Division, CARDE.

CANADIAN ARMAMENT RESEARCH AND DEVELOPMENT ESTABLISHMENT

Quebec, Que. September 1968.

TURBULENT WAKE STUDIES

ABSTRACT

Experiments ~~being~~ undertaken to investigate both the mean and fluctuating properties of turbulent wakes are described. The diagnostic techniques ~~which are~~ used to make local measurements in the wake utilize an electron beam fluorescence probe, sequential spark velocity apparatus, cooled-film anemometers, and electrostatic probe arrays. These provide measures of mass density, velocity, temperature and charge density fluctuations, as well as the means for inferring some properties of the wake turbulence. In each case some typical results are used to illustrate the capability of the techniques. Some comparisons are made between the results obtained by different experiments.

TABLE OF CONTENTS

BLANK PAGE

TURBULENT WAKE STUDIES

1.0 INTRODUCTION

The Canadian Armament Research and Development Establishment (CARDE) in cooperating with the Advanced Research Projects Agency (ARPA) has undertaken a wide-ranging program of experimental investigations of turbulent wake characteristics. These experiments are being carried out behind hypersonic projectiles in free flight in the CARDE ballistic range facilities. The emphasis of the program is on the use of local or point measurement techniques, with the objective of measuring both the mean properties of the turbulent wake and the characteristics of various turbulent fluctuations. The need for basic experimental data concerning the properties of turbulent wakes of hypersonic bodies in order to provide some foundation for further theoretical effort has been the theme of two recent review articles by Lykoudis (1,2).

1.1 THE PROGRAM

The program of wake investigation can be classified under three main headings: the operational experiments, the new experiments under development and the conventional monitoring facilities. The operational experiments involve the measurements of velocity, mass density, temperature and electron density using respectively the sequential spark, electron beam, cooled film anemometer and electrostatic probe techniques. The new experiments under development include the evaluation of wake chemistry using mass spectrometric analysis and the use of a hot filament of gas to study the turbulent transport in the wake. The conventional monitoring facilities comprise both the photographic techniques such as spark X-ray shadowgraph and optical schlieren systems as well as microwave interferometric and cavity systems.

The present paper will concern itself principaly with the main CARDE experiments. Since the CARDE program has not previously been treated as one entity in the open literature, the component parts will be described in some detail. Before beginning this discussion, a brief tour of the CARDE range facilities will be in order.

1.2 CARDE HYPERSONIC RANGE FACILITIES

Two hypersonic ballistic range facilities are being used for the turbulent wake program, these being Range 3 and Range 5.

Range 3, which is used almost exclusively for the sequential spark experiment, has a 6-foot diameter flight chamber of about 180 feet in overall length. The light gas gun launcher in use on this range has a 4-inch base diameter pump tube of 32 feet in length and a 1.5-inch diameter launch tube of 40 feet in length. This gun, using constant base pressure cycle, is capable of projecting saboted cones and spheres at velocities from 4000 to 18000 feet/second. Standard projectile base diameters on Range 3 are 1 inch for spheres and 0.7 inch for cones.

TURBULENT WAKE STUDIES

On the Range 5 facility, the flight chamber diameter is 10 feet while its length is over 400 feet (Figure 1). The 2-stage helium launcher has a 10-inch diameter pump tube of 34 feet in length while the 4-inch diameter launch tube is almost 70 feet long (Figure 2). On this range, 2.0-inch base diameter cones and 2.7-inch diameter spheres can be launched. These projectiles (Figure 3) are among the largest flown in ballistic range facilities in North America.

All projectiles are launched in sabots which support and guide the models during acceleration in the launch tubes. Sabots of various geometries fabricated from polycarbonate resin are used. Aerodynamic separation of model and sabot and mechanical deflection of sabot components are achieved in the dump tank ahead of the flight chamber itself. The dump tank is normally held at a higher pressure than that of the range tank, and mylar diaphragms are used to isolate each tank.

Standard optical techniques are used to align the gun, and to locate the sabot discard plates, and the target. These same techniques are also used in positioning the hardware of the various experiments with respect to the predicted flight axis. The actual flight trajectory down the range is determined from a series of 30° stereo X-ray shadowgraph stations. Catenary wires and plumb lines are used as references. Shadows of the model and reference lines produced by each X-ray source are recorded on single vertical X-ray films from which the position of the model can be calculated.

The X-ray stations on Range 3 are 10 feet apart while the ones on Range 5 are 30 feet apart with provision on both ranges for additional stations on cone firings. The standard instrumentation for velocity measurements is based on time counters which are triggered by the photographic (X-ray) stations. Measurements of velocity include correction for the displacement of the projectile center from the vertical reference lines as measured on the X-ray films. With this system, positional determination accuracies are 0.1 inch with 0.2 degree in attitude on Range 3, and 0.03 inch and 0.1 degree on Range 5. The accuracy of the velocity determination is to within 100 feet/second for both facilities.

Control of the degree of purity of the range atmosphere is an important consideration for certain types of experiment. As a result of several firings a large amount of carbon dust is deposited on the range walls and some remains in the atmosphere. The accumulation of carbon on the tank walls is periodically removed by steam and hand cleaning. Experience obtained with an experiment using Rayleigh scattering of a laser beam as a mass density probe has indicated the possibility of dust particles in the ambient air, and it was confirmed that these could be effectively eliminated by pumping the range to a lower pressure than desired, allowing the particles to settle, and then bleeding air into the tank to obtain the desired pressure. On

Range 3 a complete system of filtering and drying of the range atmosphere by high efficiency filtration and dehumidification units is under accelerated development to achieve a higher degree of purity of the range atmosphere. Equipment has been purchased for monitoring the dust and moisture content of the range atmosphere and this technique will be applied to Range 5 in the reasonable future. A microwave interferometer and a Fabry-Perot cavity are also planned for installation on Range 5 next summer and these monitoring instruments will serve to provide independent measurements of atmospheric purity. A high-speed framing camera has been coupled with a schlieren system to ensure the detection of small particles originating from damaged sabots which may follow the projectile down the range. Finally effort has recently been applied to determine and reduce the effects of shock waves reflected from the walls of the range tanks, using absorbent materials.

1.3 RECORDING FACILITY

Several of the techniques now in use at CARDE to make local measurements in the turbulent wake have necessitated considerable development effort because of their novelty, and this has resulted in a bias towards a method of recording which is both simple and visual. However, the recording interval for a given wake probe may exceed a period of 20 milliseconds, with the requirement of an initial time resolution of the order of a few microseconds. The ordinary oscilloscope recording using Polaroid photography has the disadvantage of providing a relatively short period of recording time when high time resolution is required. Consequently, the recording technique adopted makes use of the vertical deflection of the beam of an oscilloscope set at very low horizontal sweep velocity. The luminous spot on the tube face is focussed on a film moving parallel to the horizontal axis. The film velocity provides time resolution. Short duration persistence of the spot has been achieved by using P-16 type phosphor screens. The Wollensak WF-7 synchroballistic Fastax camera using 100 feet rolls of 35-mm 4X film easily attains velocities of 5 centimeters/millisecond. Figure 4 shows a row of oscilloscope-camera recording channels in the Range 5 recording room. The analog record on the film was initially digitized by a moving-film flying-spot-scanner reader capable of about 3-microsecond resolution. This machine has now been replaced by an automatic film reader consisting of a precision cathode ray tube and optical system together with a Programmed Data Processor (PDP-5) computer and an interface operating as a curve-follower. Speed and precision on the new reader have both been increased by a factor of five compared to the old reader, and sampling frequencies up to one megacycle are available.

2.0 EXPERIMENTAL TECHNIQUES

2.1 SEQUENTIAL SPARK EXPERIMENT

2.1.1 Description of Experimental Technique

The technique of using sequences of sparks for the

TURBULENT WAKE STUDIES

measurement of flow velocities has been treated by various authors (3,4). This technique is a quantitative flow visualization experiment which operates on a very simple principle. When an electric spark is produced between a pair of electrodes, a low resistance ionized path is created between the electrodes and appreciable ionization persists for about 0.1 millisecond. Subsequent sparks produced during this time interval will follow the ionized path made by the first spark. When a series of sparks of short duration are made across the wake of the projectile at properly selected time intervals, the ionized path due to the first spark is displaced at the velocity of the gases in the wake and each succeeding spark re-illuminates the ionized path. By open shutter photography of the spark traces, a profile of the displacement of the gas is obtained and the wake velocity can be calculated knowing the time interval between the sparks.

The instrumentation designed to produce the sparks generates 0.8-microsecond pulses at 90 kilovolts across the electrodes with a maximum current of 20 amperes in the discharge. These high-voltage pulses are sufficient to obtain with ease the formation of a spark path across gaps of 5 to 7 inches at pressures from 10 to 200 torr. The time interval between the sparks can be adjusted to any value from 3 to 150 microseconds. A typical train of pulses for velocity measurement in the wake consists of a series of four pulses at intervals of 3 microseconds in order to form the spark path, followed by a series of 4 pulses at properly selected time intervals. It was found experimentally that large curvatures of the spark path may reduce the accuracy of the measurement. These large curvatures can be avoided by a proper adjustment of the spark intervals. Satisfactory results are obtained when the wake displacement between two sparks is 10 to 20% of the viscous wake width.

With the recent development of a method to select the position of the spark in an array of electrode pairs, it is now possible to measure multiple radial profiles in the wake of the same projectile. Figure 5 shows the stereo photographs of the three sequences of sparks made in the wake of a one-inch aluminum sphere travelling at 14,300 ft/sec at ambient pressure of 40 torr. These three sequences (from left to right) in each of the stereo photographs were made at axial distances of 450, 1000, and 2400 body diameters using spark intervals of 35, 75 and 150 microseconds respectively. The switching of the spark position is made in the following way: The three anodes (top electrodes in Figure 5) are connected in parallel and the + 90 kilovolt trains of pulses are applied to the anodes. The cathodes are insulated from one another and a 10-microsecond, -30-kilovolt pulse is applied to one of the cathodes to establish a preferred position for the spark to occur between this cathode and its corresponding anode. The reliability of the spark switching depends heavily on the synchronization of the positive pulses fed to the anodes with the negative pulse on the cathode. The switching is greatly helped by the fact that between sequences, the moving wake removes the column of gas heated by the previous sparks. Switching of the spark position has been achieved with intervals as short as 0.75 millisecond between sequences.

TURBULENT WAKE STUDIES

Preliminary measurements have indicated that the sparks do not necessarily pass through the center of the wake along a straight path and therefore, a three-dimensional analysis of the spark path is required. This is achieved by a precision stereo system consisting of two cameras at 60 degrees from the flight axis together with horizontal and vertical reference lines to define the geometry. A film reader reproducing the range geometry is used to perform the three-dimensional analysis of the spark traces. The flight trajectory of the projectile with respect to the spark paths is determined to an accuracy of 0.1 inch from the X-ray shadowgraph system.

2.1.2 Data Reduction Method

An example of the data reduction procedure is given using the sequence of sparks shown in Figure 6. In this case, a series of sparks were made at a distance of 600 body diameters behind a one-inch diameter aluminum sphere travelling at 14,560 feet per second at an ambient pressure of 40 torr. The sequence of 7 sparks at 40-microsecond interval is shown together with a schlieren photograph taken immediately after the occurrence of the fourth spark. It is seen that, in this case, the diameter of the turbulent wake is greater than the electrode gap.

In order to obtain radial velocity profiles from this data, it is necessary first of all to locate accurately the flight path of the projectile with respect to the horizontal reference lines. The plates from the stereo spark cameras are then mounted in the stereo projector reading assembly which is aligned by using the vertical and horizontal reference lines. The co-ordinates of numerous points of each spark in the xz and yz planes are determined by standard photogrammetric techniques. Projections of the sparks are shown in Figure 7 where the x axis is the direction of flight, the z axis is the vertical direction and the y axis is the horizontal one. This figure also shows the displacement of three of the sparks in the yz plane and it is seen that none of them passes through the axis of the wake. This was the case for all seven sparks of this sequence. The analysis is done by measuring the distance between points on consecutive sparks and by computing the velocities using the measured time interval between the sparks. It is assumed in the analysis that the velocity in the z direction is zero.

Graphs of the resulting velocity profiles obtained from every pair of consecutive sparks are shown in Figure 8A. The notation V_{23} means the velocity profile computed from the second and third sparks. It is seen in this figure that no measurements closer than 0.3 body diameters from the axis are available because the sparks did not pass through the center of the wake. Lateral wake velocities are shown in Figure 8B, (the direction towards the cameras being positive). Profiles averaged for the total duration of the sequence for the axial and lateral wake velocity are obtained for each round and these averaged profiles are usually used for further analysis.

TURBULENT WAKE STUDIES

A considerable amount of wake velocity data has already been gathered behind one-inch diameter spheres travelling at supersonic and hypersonic velocities. Measurements behind supersonic spheres (4000 ft/sec) cover a range of axial distance from 3 to 300 body diameters at ambient pressures between 10 and 200 torr. Measurements behind hypersonic spheres (12000 - 15000 ft/sec) are spread over a range of axial distance from 150 to 1000 body diameters and a range of pressure from 20 to 76 torr. Some of this data has already been published in the literature (5,6).

2.2 ELECTROSTATIC PROBE EXPERIMENT

The use of electrostatic probes to investigate turbulent wake plasmas is somewhat unsatisfactory because of the difficulty in interpreting probe current. The requirement of having turbulence in the ballistic range prevents operation at sufficiently low pressures for the established collisionless probe theory to be applicable and an appropriate continuum theory is not available. Nevertheless it has been observed at Lincoln Laboratories (7) that the mean current to an electrostatic probe in a wake follows the mean electron density, and there is some supporting evidence from turbulent flame study at SRI (8) that a major contribution to fluctuations in probe current is due to fluctuations in charge density. Of course some results can be obtained with probes which do not depend on the interpretation of the probe current. For example in measurements of convection velocity, velocity fluctuations, and to a lesser extent, time scales of the turbulence, the electrons in the wake may be considered as a kind of passive contaminant or tracer.

The original and still the final objective of electrostatic probe work in the turbulent wake at CARDE is to measure the characteristics of electron density fluctuations. The most valuable results to date, however, have been obtained by exploring other promising avenues, in particular, velocity. Beginning with the use of single probes, it was realized that interpretation of a probe signal time history in terms of a spatial pattern would require the use of Taylor's hypothesis and a suitable mean wake velocity. Rather than rely on the results of another experiment, an attempt was made to measure wake velocity with a device consisting of two probes aligned parallel to the line of flight. When this technique gave promise of success, it was only a short series of steps to the adaption of the classical one fixed probe and one moving probe technique used to investigate turbulence in steady jets (9) to produce the electrostatic probe array technique currently in use at CARDE to investigate wake turbulence in the ballistic range (10).

Figure 9 shows a typical axial electrostatic probe array consisting of five equidistantly spaced electrostatic probes mounted in a thin support which is aligned along the flight trajectory so as to present a minimum interference to the flow. Because of dispersion the radial distance of the wake axis from the tips of the probes is determined only when the projectile is fired. After the

passage of the projectile, the wake grows onto the array. As the wake is convected past, it is seen first by the first probe in the array, then the second, third, fourth, and finally the fifth. To simplify synchronization and data reduction, the signals of each of the four last probes are recorded individually on a Fastax film along with the signal of the first probe. Figure 10 shows a typical example of the four pairs of probe signals from five probes (P_1 designates the first probe, P_2, P_3, P_4 and P_5 the following probes). The pair of signals on each film are digitized and a cross-correlation curve of each probe signal with the signal of the first is obtained.

Because of the decay of the mean wake velocity and the decay of the mean electron density in the wake, the sets of electrostatic probe signals are divided into short segments. The normal length of a correlated interval of signal is about 0.5 millisecond, which corresponds to a change of axial distance behind the projectile of about 30 body diameters. Figure 11 gives an example of a family of cross-correlation curves from a given set of probe signal segments. The envelope drawn over the four cross correlation curves represents the autocorrelation in the moving frame (9) from which a time scale measuring the temporal change of the turbulence pattern can be inferred. The points of tangency between the cross-correlation curves and the envelope measure the time lag arising before the pattern which first passed the first probe P_1 arrives at successive probes. By plotting the distance between pairs of probes as a function of the time lags obtained corresponding to the various points of tangency, we arrive at a curve such as the one given in Figure 12. The slope of the straight line fitting the points is a measure of the convection velocity of the wake past the array of probes. Successive sets of signal segments provide successive estimates of the velocity history along the wake at a given radial distance, thereby allowing a complete profile of normalized wake velocity versus axial distance to be plotted.

Space correlation data has also been obtained from the probe array signals. In this paper, however, this data will be overlooked to concentrate on the velocity results and their comparison with the data obtained from the sequential spark technique.

2.3 COOLED-FILM ANEMOMETER EXPERIMENT

The first application of hot wire anemometry to the study of the turbulent characteristics of projectiles in free flight was made by Fox, et al (11), employing a constant temperature anemometer to study the wake of 0.22 calibre rifle bullets travelling at supersonic speed in a ballistic range. These measurements were aimed primarily at determining the frequency content of the wake and from the measured power spectral density they inferred the micro scale and integral scale of the turbulence as functions of axial distance downstream.

In the hypersonic wake the environmental temperature may exceed the operating temperature of conventional hot wires and it

becomes attractive to consider the use of the cooled-film anemometer developed by Fingerson (12). The experimental technique in use at CARDE is an application of the two-temperature method, where two anemometers are employed to determine both temperature and velocity.

In the cooled-film constant temperature anemometer, the sensing element consists of a tiny pyrex-U-tube, 0.006" in diameter, through which a cooling fluid can be circulated. A platinum film, one micron thick and 0.040" long, is deposited on one limb of the U-tube and electrical contact is provided by a gold coating on the rest of the tube (Figure 13). With the coolant circulating through the sensor, the platinum film is maintained at constant resistance (and hence constant temperature) by means of a bridge circuit (of which the sensor forms a branch) and a feedback system.

In the absence of any heat transfer between the film and the environment, the electrical power supplied to the film element is dissipated by the coolant circulating through the sensor. When this element is exposed to environmental conditions such that a power transfer between the environment and the element occurs, the power supplied to the element by the heat flux system is adjusted so that the power dissipation to the coolant is unaltered (Figure 13). In this way fluctuations in bridge voltage are related to changes in the environmental conditions.

For the determination of wake temperature and velocity histories, the two-temperature method is employed. Two sensing elements, each controlled by its own heat flux system, are placed in close proximity to each other and to the predicted flight path of the projectile. The sensing elements are maintained at two different but constant temperatures and the two outputs are recorded simultaneously on the same Fastax film. The signals from the two probes can then be analysed to yield wake temperature and velocity as functions of distance behind the projectile.

The analysis involves the use of an empirical relation between Nusselt Number, N_u, and Reynolds number, R_e, of the probe cylinder, and the assumption of constant pressure wake. One such relationship which may be employed is that due to Collis and Williams (13) which was obtained for the cooling of heated cylinders at relatively low environment temperatures and under subsonic incompressible flow conditions in undissociated air. This relationship reads

$$Nu_f \left(\frac{T_e}{T_f}\right)^m = a + b\,(Re_f)^n \qquad (1)$$

where subscript f refers to film conditions (the film temperature T_f is usually taken as the mean of the sensor and environment temperatures),

TURBULENT WAKE STUDIES

T_e is the environment temperature and a, b, m and n, are empirical constants as given below

Re_f	a	b	m	n
0.02-44	0.24	0.56	0.17	0.45
44-140	0	0.48	0.17	0.51

Substituting for the quantities in equation (1) we obtain

$$V = \frac{\nu_f}{d}\left[\frac{1}{b}\left\{\frac{Q}{\pi \ell \; k_f (T_e - T_s) - 2\frac{k_f}{k_s} k_n Q}\left(\frac{T_f}{T_e}\right)^m - a\right\}\right]^{\frac{1}{n}} \qquad (2)$$

where V is the fluid velocity past the sensor,
d is the cylinder diameter,
ℓ is the cylinder length,
k_f is the thermal conductivity of the environment fluid, evaluated at film temperature, T_f,
k_s is the thermal conductivity of the environment fluid, evaluated at sensor temperature, T_s,
λ_s is the mean free path of the environment fluid at sensor temperature, T_s,
Q is the power transfer from the environment to the sensor.
$k_n = \frac{\lambda_s}{d}$ is the Knudsen number evaluated at sensor temperature.

For two sensors operating at the same point in the fluid, but at different constant temperatures denoted by subscripts 1 and 2, two equations of the form of Eq. (2) pertain. The velocity V may be eliminated between them and the resulting equation solved for the environment temperature T_e. An iterative technique for solution of the equations has been described by Ellington and Trottier (14) and the method programmed for solution using a digital computer. A pair of values (T_e, V) is computed from each input pair (Q_1, Q_2).

It became evident at an early stage that the method suffered from inaccuracies introduced in the calibration, measurement, recording, reading and analysis phases of the experiment. These inaccuracies were such as to produce an unacceptably large cumulative error in the final determination of wake temperature and velocity. For ease of performing an error analysis Eq. (2) can be written in a simplified form as

$$Q_1 = (T_e - T_{s_1})\left(\frac{V}{Z_1}\right)^{\frac{1}{2}} \qquad (3)$$

$$Q_2 = (T_e - T_{s_2})\left(\frac{V}{Z_2}\right)^{\frac{1}{2}} \qquad (4)$$

for the two sensors respectively corresponding to the Collis and Williams correlation for $44 < Re_f < 140$. $Z_{1,2}$ is defined

$$Z_{1,2} = \frac{\nu_{f_{1,2}}}{d_{1,2}\, b^2\, \pi^2\, \ell_{1,2}^2\, k^2 f_{1,2} \left(\frac{T_{f_{1,2}}}{T_e}\right)^{0.34}} . \qquad (5)$$

For a given ambient pressure, over the range of realizable values of T_{s_1}, and T_{s_2}, the values of Z do not vary by more than a few percent for typical values of T_e likely to be encountered in the hypersonic wake. Thus we take:

$$Z_1 = Z_2 = Z, \text{ say}.$$

From equations (3) and (4) we obtain

$$T_e = \frac{K T_{s_2} - T_{s_1}}{K - 1} \qquad (6)$$

and,

$$V = \frac{Z Q_2^2 (K-1)^2}{(T_{s_2} - T_{s_1})^2} \qquad (7)$$

where we have defined the parameter K,

$$K = \frac{Q_1}{Q_2} = \frac{T_e - T_{s_1}}{T_e - T_{s_2}} \qquad (8)$$

The fractional error in K is related to fractional error in Q_1 and Q_2. Assuming $\Delta Q_1/Q_2 = \Delta Q_2/Q_2 = \Delta Q/Q$ we note that the maximum error in K occurs when

$$\frac{\Delta Q}{Q} = -\Delta Q_1/Q_1 = \Delta Q_2/Q_2 .$$

The resultant errors in T_2 and V are given by

$$\Delta \frac{T_e}{T_e} = \pm 2 \frac{\Delta Q}{Q} \left(\frac{K T_{s_2}}{K T_{s_2} - T_{s_1}} - \frac{K}{K-1} \right) \qquad (9)$$

and

$$\frac{\Delta V}{V} = \pm 2 \frac{\Delta Q}{Q} \left(\frac{K - 1}{K - 1} \right) \qquad (10)$$

TURBULENT WAKE STUDIES

Equations 9 and 10 have been evaluated as functions of K for various combinations of sensor temperatures. Figure 14 is appropriate to sensor temperatures T_{s1} = 400° and T_{s2} = 700°k. It will be seen that the values $(\Delta T_e/T_e)/(\Delta Q/Q)$ increase sharply for values of K less than 2.

With distilled water coolant and laminar coolant flow in the sensor, sensor temperatures are restricted from 350°K to 450°K. Under hypersonic wake environmental conditions of T_e = 1000°K, and T_{s1} = 400° and T_{s2} = 500°K, the maximum realizable value of K is about 1.2. Under these conditions, the results of an error analysis show that a 10% error in the measured heat transfer signals can result in a maximum error in estimated wake temperature of 60% and a maximum error in estimated wake velocity of 220%. The corresponding figures for T_{s1} = 600°K, T_{s2} = 800°K, T_e = 1000°K are 8% and 60% on temperature and velocity respectively, corresponding to a 10% error in measured signal.

Consequently, some effort has been expended to increase the maximum operating sensor temperature and also to improve the accuracy of the measurement. With regard to the former, it has been found that with the use of a coolant of higher viscosity than that of water, the mass flow of coolant can be increased to accomodate a higher sensor temperature before the coolant flow becomes turbulent. Temperatures in excess of 800°K have been obtained in this way, with the use of fluids such as Fluorolube FS.

The use of fluorolube in one of the sensors also permits the power dissipation to the coolant to be equalized for the two sensors. This is necessary, because as can be shown analytically (15) the frequency response of the system is proportional to the power dissipation to the coolant.

Trials have been made using sensor temperatures of 400°K (water coolant) and 700°K (Fluorolube). Under these circumstances the frequency response of the two sensors is reasonably matched. Some typical raw data signals are shown in Figure 15.

Figure 16 shows temperature results using the two-temperature method in the inviscid region of the wake and in the viscous core. Although the mean temperature values are probably reasonable the fluctuations observed are still subject to question. It has been decided that further progress in this technique will require the additional precision capability of digital data recording now under procurement.

2.4 ELECTRON BEAM EXPERIMENT

The principle of operation of the electron beam experiment is as follows: when a beam of electrons traverses low density air, a small number of electrons collide with nitrogen molecules leaving the nitrogen in an excited state. The intense fluorescence released

by the almost instantaneous deexcitation is well defined within the width of the beam of electrons. The intensity of the fluorescence is then a measure of the gas density in any small volume from which the fluorescence is observed. At gas densities low enough to prevent non-radiative deexcitation processes, the light output is a linear function of gas density and electron beam current.

This technique which has been successfully used in the study of densities in shock tubes and shock tunnels (16, 17, 18) is most appropriate for the measurement of mass density in the wakes of hypersonic projectiles because the probe is capable of temporal and spatial resolution without mechanically interfering with the wake flow. As the beam electrons are attenuated and scattered by oxygen and nitrogen molecules, ambient pressures (densities) are restricted to less than 10 torr. This pressure limitation permits measurements of average density in both laminar and turbulent regimes but reduces the capability of the probe to measure fluctuations at densities corresponding to the turbulent regime.

A detailed analysis of the excitation emission processes was reported by Muntz (19) and Davidson and O'Neill (20) have made a complete spectrographic study of the radiation. The bulk of radiation is emitted by the second positive system of the neutral nitrogen molecule N_2 $(2+)$ and by the first negative system of the singly ionized nitrogen N_2 $(1-)$. For pressures above one torr which are of most interest, the intensity is found to be both stronger and more linear from the N_2 $(2+)$ system than that from the $N_2^+(1-)$. Tests conducted in pure nitrogen at pressures up to 10 torr have shown that the intensity of the N_2 $(2+)$ system is more linearly dependent than is the case in air.

The density measuring apparatus is illustrated in Figure 17. The 100 Kev beam generator, capable of a beam current of one milliampere has multiple pumping stages allowing operation at test section pressures up to 10 torr. The light collecting and field defining system consists of a quartz lens and a slit defining a 1.2 mm by 12 mm field of view with its smaller dimension along the beam direction. The photodetector thus measures the fluorescence originating in a cylindrical volume geometrically defined by the field of view and the beam diameter and spectrally limited by an interference filter centered at 3375Å with bandwidth of 55Å and a transmission of 45%.

Calibration under static conditions at room temperature and various nitrogen pressures ranging from 0.5 to 10 torr has shown some departure from an exact linear dependence. The calibration data can be fitted by

$$S = k \frac{a\rho}{a\rho} \qquad (11)$$

where S is the output signal from the photodetector
k is a normalizing factor
a is a parameter to fit the curve shape
ρ is the gas density.

TURBULENT WAKE STUDIES

By a least mean squares fit of the calibration data points over equation (11) the value of "a" can be determined. The determination of the normalizing factor "k" is more difficult as this value depends on various experimental and instrumental parameters such as the solid angle of the light collecting system, amplifier gain and detector sensitivity, as well as filter and lens transmission. However, k can be determined by measuring the fluorescence intensity under ambient conditions just prior to the arrival of the projectile. Then we have

$$S_\infty = k \frac{a\rho_\infty}{a+\rho_\infty} \qquad (12)$$

and the density ratio normalized to ambient conditions becomes

$$\rho/\rho_\infty = \frac{aS}{\rho_\infty(ka-S)} \qquad (13)$$

where k is determined by equation (12).

The parameter "a" which is related to the quenching efficiency of the gas may have a temperature dependence. Shock tube results of Camac (21) have shown the temperature effect to be negligible at all temperatures of interest here.

Typical density measurements of relative wake density versus downstream distance are shown in Figure 18. These densities are measured along the axis of wakes of 2.7-inch diameter titanium sphere fired at 15000 ft/sec in nitrogen and air atmosphere at 8.0 torr. Recent wake density computations performed by K.S. Wen (22) allowing variable diffusivity along the turbulent wake have shown excellent agreement with these experimental axial wake density results for axial distances from 10 to 1000 body diameters.

3.0 MEAN CHARACTERISTICS OF THE TURBULENT WAKE

The determination of the mean characteristics of the turbulent wake is of primary importance in the verification of a theoretical model of the wake. The four main wake experiments described above are designed to yield mean distributions of mass density, temperature and velocity. The determination of these mean characteristics, however, requires a statistically reasonable amount of data. Most of the data available at the present time was gathered at the same time as refinements were still being made to the experimental techniques. The data also usually covers a large number of ambient conditions so that it is difficult to extract accurate mean characteristics of the wake. Consequently the discussion on mean wake characteristics will be limited to velocity where data obtained by the sequential spark technique can be compared to the convection velocities obtained from the cross correlation of the signals collected by axial arrays of electrostatic probes.

TURBULENT WAKE STUDIES

3.1 SEMI LOGARITHMIC DECAY OF WAKE VELOCITY

Wake velocity data from the sequential spark experiment is in the form of radial velocity profiles at fixed axial distances in the wake. Convection velocities from the electrostatic probe array experiment, on the other hand, are obtained in the form of axial velocity profiles at a fixed distance from the axis of the wake. In order to permit comparison of the experimental results from the two techniques, a large number of radial velocity profiles at various axial distances as measured by the spark technique were transformed into axial profiles in the following way: the normalized mean velocity values of each radial profile are plotted and linear interpolation is made between data points of the mean curve to obtain velocity data at fixed radial distances, say, 0.1, 0.2, 0.3, 0.4, etc., body diameters. The axial distributions of data points thus obtained can be compared directly with the axial distributions of data points obtained by the probe array at the same radial distance. Because of the large scatter in the sequential spark data due to turbulence which masks differences resulting from various ambient conditions, relatively large variations in ambient conditions have been tolerated in the data used to obtain the axial distributions of velocity, in order to increase the statistical accuracy. Radial profiles measured behind spheres travelling at velocities between 12,000 and 15,000 ft/sec were used because the normalized wake velocity shows a very weak dependence on projectile velocity in that range of velocities. Measurements made at pressures varying between 20 and 76 torr have been utilized despite the appreciable dependence of the wake velocity on pressure. Assuming a linear dependence of wake velocity on ambient pressure, however, the distribution of data points is reasonably balanced giving an average pressure of 40 torr. A total of forty radial profiles were used in the formation of these distributions of points. A least mean square fit of an equation of the form

$$V_w/V_\infty = a + b \log X/D, \qquad (14)$$

where a and b are functions of radial position, was made on the distribution of velocity data points at each preselected radial distance. This particular form of equation has no theoretical justification and the best reason for using it is that it fits the data very well. Figure 19 shows a typical example of the semi-logarithmic least mean square fit (open circles and full line) of the sequential spark wake velocity data at a radial distance of 0.7 body diameter. Only relative importance should be attached to the scatter of the data points because of the large range of ambient conditions pertinent to these data. The wake velocity data cover a range of axial distance from 130 to 1000 body diameters. For purposes of comparison, Figure 19 also shows a least mean square fit of wake velocity data obtained from the electrostatic probe array technique behind a 2.7-inch Titanium sphere travelling at 15000 ft/sec at an ambient pressure of 20 torr (black circles and dotted line). The scatter of the probe array data points is typical of the velocity fluctuations that can be observed on a single measurement of an axial

velocity profile. More measurements in the same conditions may increase the scatter, however, the agreement between the results obtained by the sequential spark and the probe array techniques is remarkably good.

Figure 20 shows a family of mean axial wake velocity profiles obtained from semi-logarithmic fits of the sequential spark data. Profiles are given at every 0.2 body diameter between 0.4 and 2.0 body diameters of radial distance. For values of normalized radial distance (R/D) smaller than 0.4 and larger than 2.0 body diameters, the number of data points in the distribution is too small to obtain statistical accuracy in the least mean square fit of the data. The decrease in the number of data points at small R/D is due to the fact that the spark often passes at some distance from the wake axis. At large R/D, the decrease is either due to the width of the moving core of the wake, or to the relatively small separation of 5½ inches between the electrodes. It can be seen in Figure 20 that the slope of the axial profiles decreases fairly smoothly with radial distance and that all the profiles converge to an almost common value of $V_w/V_\infty = .03$ at an axial distance of 1000 body diameters.

3.2 POWER LAW DECAY OF WAKE VELOCITY

There is more theoretical justification for plotting the velocity decay data on a log-log scale, and looking for a power law type fit. It has been shown by Townsend (23) that in the case of the incompressible "self-preserving" axisymmetric turbulent wake, the growth of the viscous core varies as the 1/3 power of the distance behind the body, while the decay of the wake velocity varies as the minus 2/3 power of the distance. For the hypersonic turbulent wake, there is a large amount of wake growth data (24, 25) to show that the 1/3 power law is obeyed over a range of axial distance from 100 to 10,000 body diameters behind a body. Least mean square fits of an equation of the form

$$V_w/V_\infty = C_1 (X/D)^{C_2} \qquad (15)$$

were made on the distributions of sequential spark velocity data points previously used for the semi-logarithmic fits. Data points obtained at axial distances smaller than 300 body diameters have been neglected in order to reduce the range of axial distance since the distributions of data points at small X/D tends to deviate somewhat from the power law particularly at small radial distance ($R/D < 1.0$ body diameter). Figure 21 shows a typical plot of sequential spark data and least mean square fitted curve (open points and full line) at a radial distance of 1.2 body diameter. Also shown (solid points) are probe array results obtained behind a 2.7 inch sphere at 15000 ft/sec and 20 torr and the corresponding least mean squares fit (dotted line). The agreement between the two least mean square curves is very good. The slope of the sequential spark curve is minus unity while the probe array data indicate a slope of 0.9. The scatter of the velocity data points for both sets of data is

appreciably larger at R/D = 1.2 body diameters (Figure 21) than at R/D = 0.7 body diameter (Figure 19) because the radial velocity profile is relatively flat at R/D = 1.2 body diameters (6).

Figure 22 shows a family of mean axial wake velocity profiles obtained from the least mean square fit of equation 15 on the sequential spark data. The slope of the axial profiles decreases gradually from minus 1.2 at R/D = 0.4 body diameter to minus 0.4 at R/D = 2.4 body diameters.

3.3 WAKE VELOCITY DEPENDENCE ON REYNOLDS NUMBER

Both the electrostatic probe array and sequential spark results indicate an appreciable dependence of the wake velocity on Reynolds number, or more specifically on ambient pressure times body size. Figure 23 shows probe array velocity results obtained in the wake of one inch spheres (solid circles) and of 2.7 inch spheres (open circles) at a pressure of 20 torr and at velocity from 14000 to 15500 feet/second. These results are compared with semi-logarithmic fits of sequential spark data. The results indicate that the electrostatic probe array data obtained behind the 2.7 inch spheres (P_∞ D = 135 torr-cm) are in consistent agreement with the sequential spark curves (average P_∞ D = 100 torr-cm). On the other hand, the probe data obtained behind one inch spheres (P_∞ D = 50 torr-cm) lie consistently low with respect to the 135 torr-cm data (26).

Further evidence of the dependence of wake velocity on Reynolds number can be seen in Figure 24A and 25A showing the mean radial profiles obtained from measurements at the same projectile velocity (15000 ft/sec) and axial distance (X/D = 1000 B.D.) and for pressures of 20 and 76 torr. At 20 torr the normalized velocity on the axis is 0.021 while at 76 torr, this value is 0.026.

4.0 FLUCTUATING CHARACTERISTICS OF THE TURBULENT WAKE

The distributions of data points in Figures 19 and 21 show an appreciable scatter which can be mainly attributed to turbulent fluctuations. In this section, estimates of the turbulence intensity of the wake velocity will be given. An attempt to measure a characteristic time scale for turbulence will be briefly described and preliminary results will be compared with moving frame autocorrelation time scales obtained from cross correlation results of axial electrostatic probe array signals.

4.1 WAKE VELOCITY FLUCTUATION INTENSITY

Estimates of turbulent intensity can be obtained from the sequential spark experiment by collecting a certain number of radial velocity profiles under the same ambient conditions. From these measurements, a mean profile can be extracted and the standard deviation of these profiles from the mean is a measure of the turbulent intensity. Measurements in the inviscid region of the wake

of supersonic spheres have shown the repeatability of the measurement technique in the absence of turbulence (6), so that the fluctuations observed in turbulent wake measurements can be attributed in large part to turbulence.

Figure 24A shows the mean radial profiles of axial and lateral wake velocity obtained from 11 profiles measured at 1000 body diameters behind one inch spheres travelling at 15000 ft/sec in an ambient pressure of 20 torr. The mean lateral velocity profile V_{yw}/V_∞ is gratifyingly close to zero. Figure 24B shows the intensity of the velocity fluctuation as a function of radial distance. The standard deviation has been normalized to the mean axial wake velocity on the axis (R/D = 0). The value used for normalization is $V_{wo}/V_\infty = 0.021$. A turbulence intensity level varying between 10 and 20% is observed. Figure 25 shows similar results obtained from 6 measurements under conditions identical to those appropriate to the results of Figure 24 except that the pressure is 76 torr. Because of the smaller amount of data, the mean lateral velocity does not average as close as before. In this case, a value of $V_{wo}/V_\infty = 0.026$ has been used to normalize the standard deviation. The fluctuation level is comparable to that observed at 20 torr.

Similar estimates of "turbulence intensity" can be made from the electrostatic probe array data. Taking the results from an individual firing, a semi-log mean square fit of V_w/V_∞ versus X/D was obtained. Using this fit, the r.m.s. deviation of the points from the fitted curve in each of four ranges of axial distance were obtained (X/D $<$ 300, 300 - 600, 600 - 900 and 900 - 1200). The number of points in each band of axial distance is quite small, which leads to quite a large scatter in the results. Therefore the results of a large number of firings (for $1.0 \leq R/D \leq 1.5$) were averaged to obtain a mean rms velocity fluctuation v'/V_∞ (Figure 26) and also a mean local wake velocity $\bar{V}w/V_\infty$ (for $1.0 \leq R/D \leq 1.5$). From these two curves, $v'/\bar{V}w$ was computed to estimate the intensity of turbulence. The rms velocity fluctuation (v') was also normalized to the wake velocity value at the wake axis using the sequential spark estimate of Vwo. All these results are plotted in Figure 28, which shows the turbulence intensity to be of the order of 20 to 30%.

4.2 CHARACTERISTIC TIME SCALE FOR TURBULENCE

The study of turbulent mixing is generally based on the measurement of the time required for a given configuration or pattern of turbulence to be replaced by a non-correlated turbulent pattern. The time history of electrostatic probe signals yield a measure of turbulence decay at a localized spot but it seems interesting to study the time decay of a known pattern.

To produce this pattern, a series of 7 closely spaced (4μ seconds) sparks of short duration ($.8\mu$ sec) are used to form a hot filament of gas in the wake. The filament is photographed with the fast framing camera of a schlieren system. At a downstream

distance of 1200 body diameters the filament is distinctly observed for 7 to 12 frames before degradation of the pattern due to mixing in the turbulent wake renders it undetectable. Figure 27 gives a typical sequence of schlieren photographs. In order to define a criterion to obtain the decay of the pattern, each photograph was scanned by a microdensitometer in a direction parallel to the flight axis. Preliminary tests have shown that a scanning field of two body diameters in height enhances the spark definition by averaging the background fluctuation. Typical microdensitometer traces are given in Fig 28 showing the background fluctuation as well as the spark amplitude. Figure 29 shows the decay of the average peak amplitude of the spark compared with the average peak amplitude of the background, both amplitudes being averaged over a frequency band corresponding to the spark frequency.

A characteristic time scale can be obtained from the moving frame autocorrelation associated with the family of cross correlation curves obtained from the axial electrostatic probe array signals as shown in Figure 11. The time at which the moving frame autocorrelation has decreased to a value of exp (-1) is taken as an integral time scale. Figure 30 shows examples of time scales measured by the axial array probe technique in the wake of 2.7 inch spheres at 15000 ft/sec and 1.0 to 1.2 body diameters off axis for ambient pressures of 7, 20 and 76 torr. The time scales at an axial distance between 100 and 400 body diameters are appreciably longer for a pressure of 7 torr (Figure 30A) than for pressures of 20 and 76 torr (Figures 30B and C respectively). (However, the differences apparent in the trend of the results at 7 torr and at 20 and 76 torr cannot be judged significant on the basis of one or two rounds).

Only a few trials have been made with the hot filament technique. Despite the difference in resolution and criteria between the filament and array techniques, it would appear that the "time scales" obtained by the two methods are in coarse agreement.

5.0 CONCLUSIONS

An outline of the experimental investigation of the turbulent wake of hypersonic projectiles being undertaken at CARDE using ballistic range facilities in the joint CARDE-ARPA program has been presented. The main experiments in the program for observing local variations of velocity, mass density, temperature and electron density have been described in some detail, and a few typical results presented. Definitive data have not yet been produced in the case of every experiment, but a considerable amount of information has been amassed on velocity, using the sequential spark technique. This data has been presented on mean velocity profiles in the wakes of hypersonic spheres, and the close agreement between sequential spark results and velocity data from arrays of electrostatic probes has been demonstrated. Preliminary estimates of the level of velocity fluctuations in the wake as obtained from the sequential spark experiment and by the probe arrays have shown good agreement.

TURBULENT WAKE STUDIES

ACKNOWLEDGEMENTS

The success of any program for the investigation of the turbulent wake behind hypersonic projectiles in a ballistic range is dependent on the efforts and activities of a large number of operating and support personnel. The authors would express their appreciation to the members of Range Engineering Section under Mr. P. Solnoky, to the members of Range Instrumentation Section under Dr. E.G. Leger and particularly to their colleagues in Hypersonic Physics who support, carry out, and direct the experimental programs which have been described here.

Special acknowledgement is due to Mr. D. Ellington for permission to present examples of data (Figures 15 and 16) typical of that recently obtained on his cooled film anemometer experiment.

Finally the authors would acknowledge the direction and support of Dr. A. Lemay, Mr. M. Letarte and of Mr. G.H. Tidy, Director of Aerophysics Division, CARDE.

REFERENCES

1. Lykoudis, P.S. "A Review of Hypersonic Wake Studies," AIAA Journal 4, pp 577-590 April 1966.

2. Lykoudis, P.S. "Recent Developments in the Fluid Mechanics of Hypersonic Wakes." Paper presented at the XVIIth International Aeronautical Congress Madrid Oct/66.

3. Bomelburg, H.J., Herzog, J. and Weske, J.R. "The Electric Spark Method for Quantitative Measurements in Flowing Gases." AFOSR TN-59-273, ASTIA AD212707, University of Maryland 1959, Unclassified.

4. Frungel, F.B.A. "High Speed Pulse Technology" Vol II Academic Press New York 1956, pp 162-182.

5. Lahaye, C., Léger, E.G. and Lemay, A. "Radial and Axial Velocity Profiles of Hypersonic and Supersonic Wakes Measured by the Sequential Spark Method." Conference Proceeding No. 19 of the AGARD Specialists Meeting on the Fluid Physics of Hypersonic Wakes, Colorado University, May 1967.

6. Lahaye, C., Léger, E.G. and Lemay, A. "Wake Velocity Measurements Using a Sequence of Sparks." AIAA Journal Vol, No.12, pp 2274-76, December 1967.

7. Slattery, R.E., Private Communication, 1967.

8. Guthart, H., Weissman, D.E. and Morita, T., "Measurements of the Charged Particles of an Equilibrium Turbulent Plasma," Physics of Fluids, Vol 9, No. 9, 1766-1772, September 1966.

TURBULENT WAKE STUDIES

REFERENCES (CONT'D)

9. Fisher, H.J. and Davies, P.O.A.L. "Correlation Measurements in a Non-Frozen Pattern of Turbulence," J. Fluid Mech. 18, pp 97-116 January 1964.

10. Kirkpatrick, A., Heckman, D. and Cantin, A.. "Wake Plasma Turbulence Study using an Electrostatic Probe Array," AIAA Journal, Vol 5, No. 8, 1494-95, August, 1967.

11. Fox, J., Webb, W.H., Jones, B.G. and Hammit, A.G. "Hot Wire Measurements of Wake Turbulence in a Ballistic Range." AIAA Journal 5, No. 1, pp 99-102 January 1967.

12. Fingerson, L. "Instruction Manual, Heat Flux System Model 1000A." Thermosystems Inc., St. Paul Minn.

13. Collis, D.C. and William, M.J. "Two Dimensional Convections from Heated Wires at Low Reynolds Numbers." J. Fluid Mech 6, 3, pp 357-384 October 1959.

14. Ellington, D. and Trottier, G. "Studies of Turbulence in the Wakes of Hypersonic Spheres under Simulated Reentry Conditions." AGARD Conference Proceeding No. 19, Vol 2, May 1967.

15. Ellington, D. and Trottier, G., Private Communication.

16. Muntz, E.P. and Marsden, D.J. "Electron Excitation Applied to the Experimental Investigation of Rarefied Gas Flows." Third International Rarefied Gas Dynamics Symposium (J.A. Laurmann, ed.) Vol II pp 495-526, 1963 Academic Press Inc. New York, N.Y.

17. Muntz, E.P. and Softley, E.S. "A Study of Laminar Near Wakes." AIAA Journal Vol 4, No. 6, pp 961-968, June 1966.

18. Rothe, D.E. "Electron Beam Studies of the Diffusive Separation of Helium-Argon Mixtures in Free Jets and Shock Waves." UTIAS Report No. 114, July 1966, Institute for Aerospace Studies, University of Toronto, Toronto, Canada.

19. Muntz, E.P. "Measurements of Rotational Temperature, Vibrational Temperature and Molecule Concentration in Non Radiating Flows of Low Density Nitrogen." UTIA Report No. 71 April 1961.

20. Davidson, G. and O'Neill, R. "The Fluorescence of Air and Nitrogen Excited by 50 Kev Electrons." Air Force Cambridge Research Lab. AFCRL-64-466 May 1964.

21. Camac, M., AVCO Everett Res. Lab. Private Communication. Nov/66.

22. Wen, K.S. General Motors, A.C. Defence Research Laboratory Santa Barbara, Calif. Private Communication, February 1968.

TURBULENT WAKE STUDIES

REFERENCES (CONT'D)

23. Townsend, A.A. "The Structure of Turbulent Shear Flow." (Cambridge University Press), Cambridge, England, 1956, Chapter VII, pp 169-171.

24. Lyons, W.C., Brady, J.J. and Levensteins, Z.J. "Hypersonic Drag, Stability and Wake Data for Cones and Spheres." AIAA Journal, Vol 2, No. 11, pp 1948-1956, November 1964.

25. Clay, W.G., Labitt, M. and Slattery, R.E. "Measured Transition from Laminar to Turbulent Flow and Subsequent Growth of Turbulent Wakes." AIAA Journal, Vol 3, No. 5, pp 837-841, May 1965.

26. Heckman, D., Cantin, A., Emond, A. and Kirkpatrick, A. "Convection Velocity Measurements in Hypersonic Spheres Wakes." AIAA Journal Vol 6, No. 4, 750-52 April 1968.

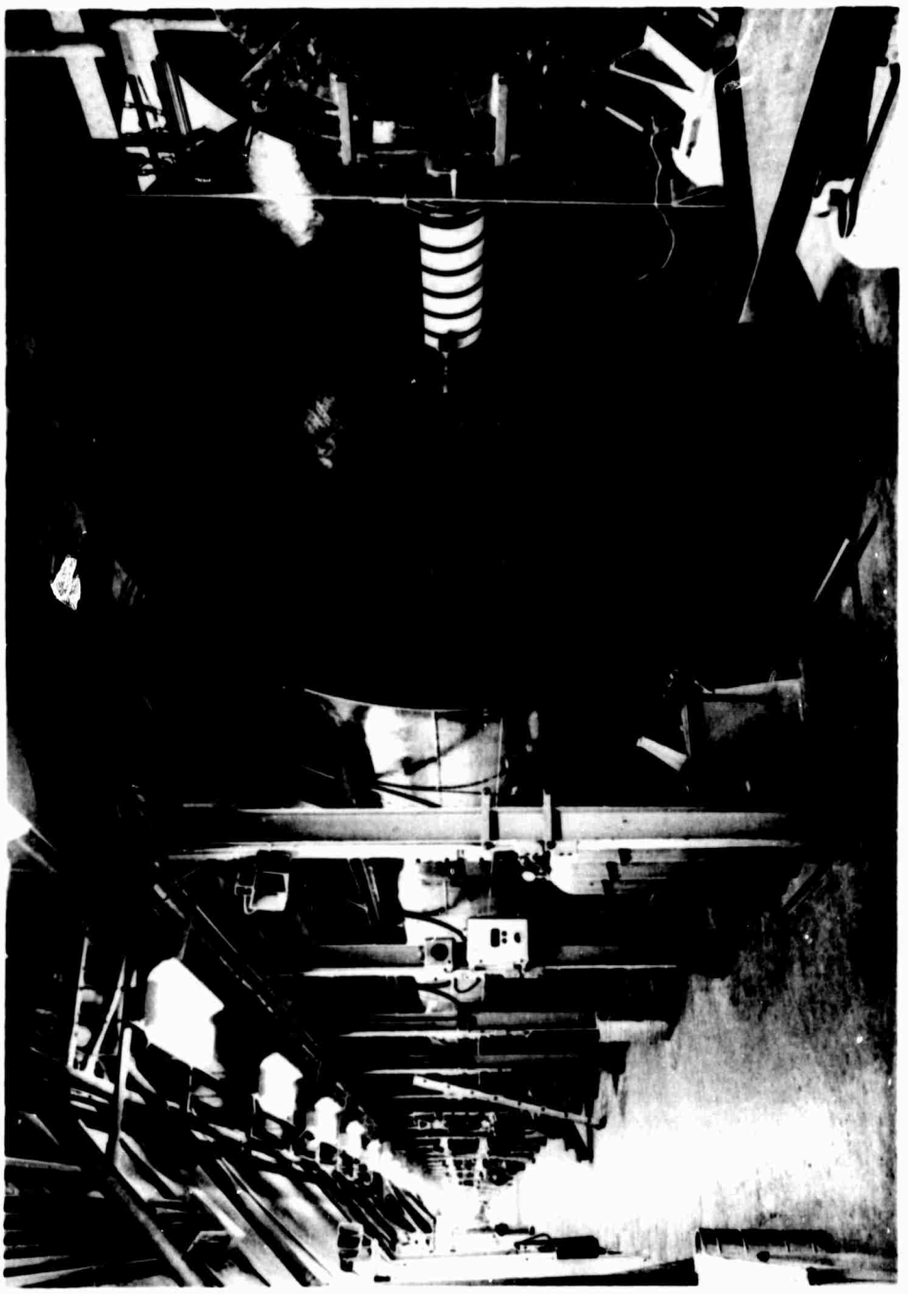

FIGURE 1 - Range No. 5 flight chamber.

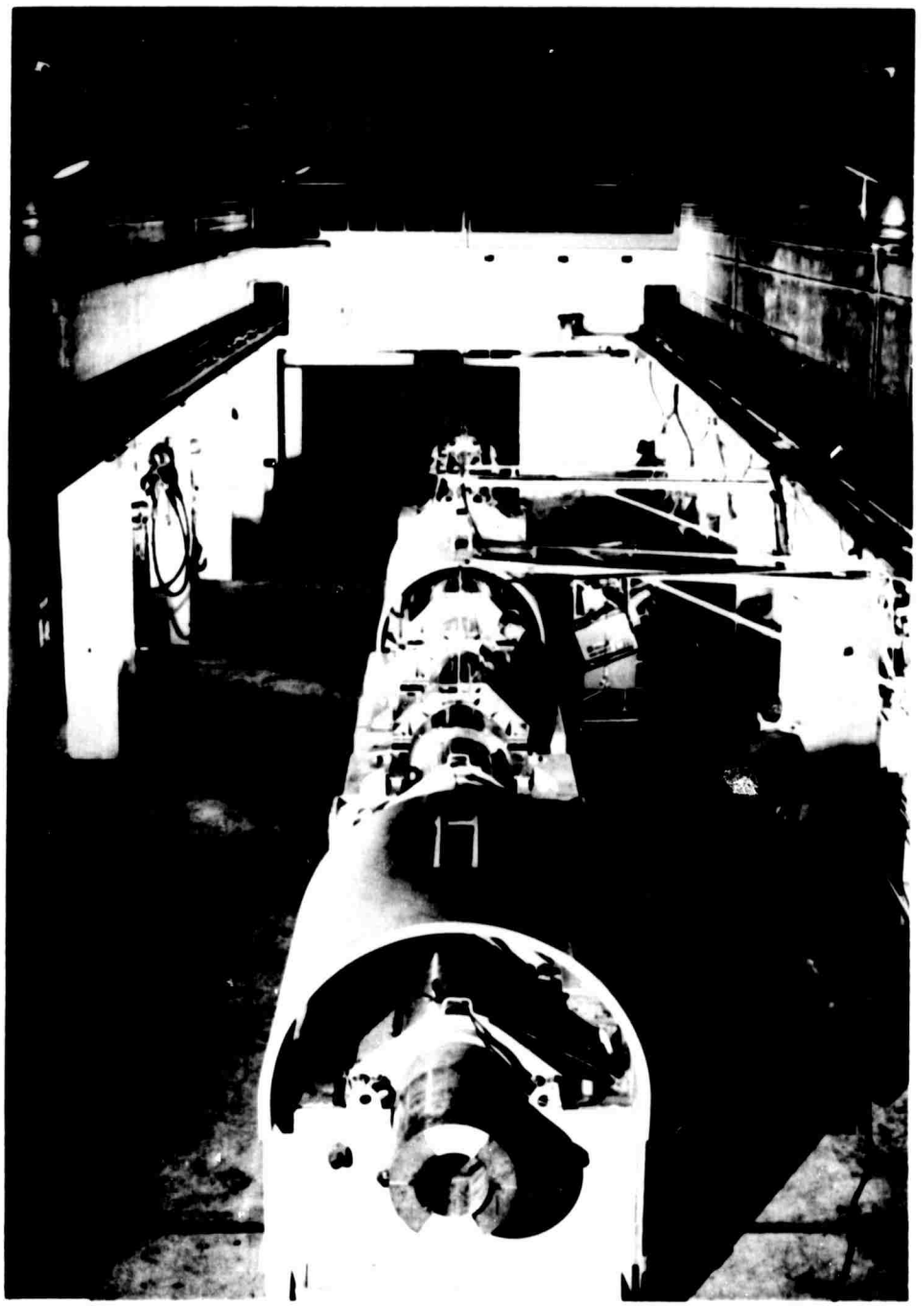

FIGURE 2 - Four inch light gas gun launcher on Range No. 5.

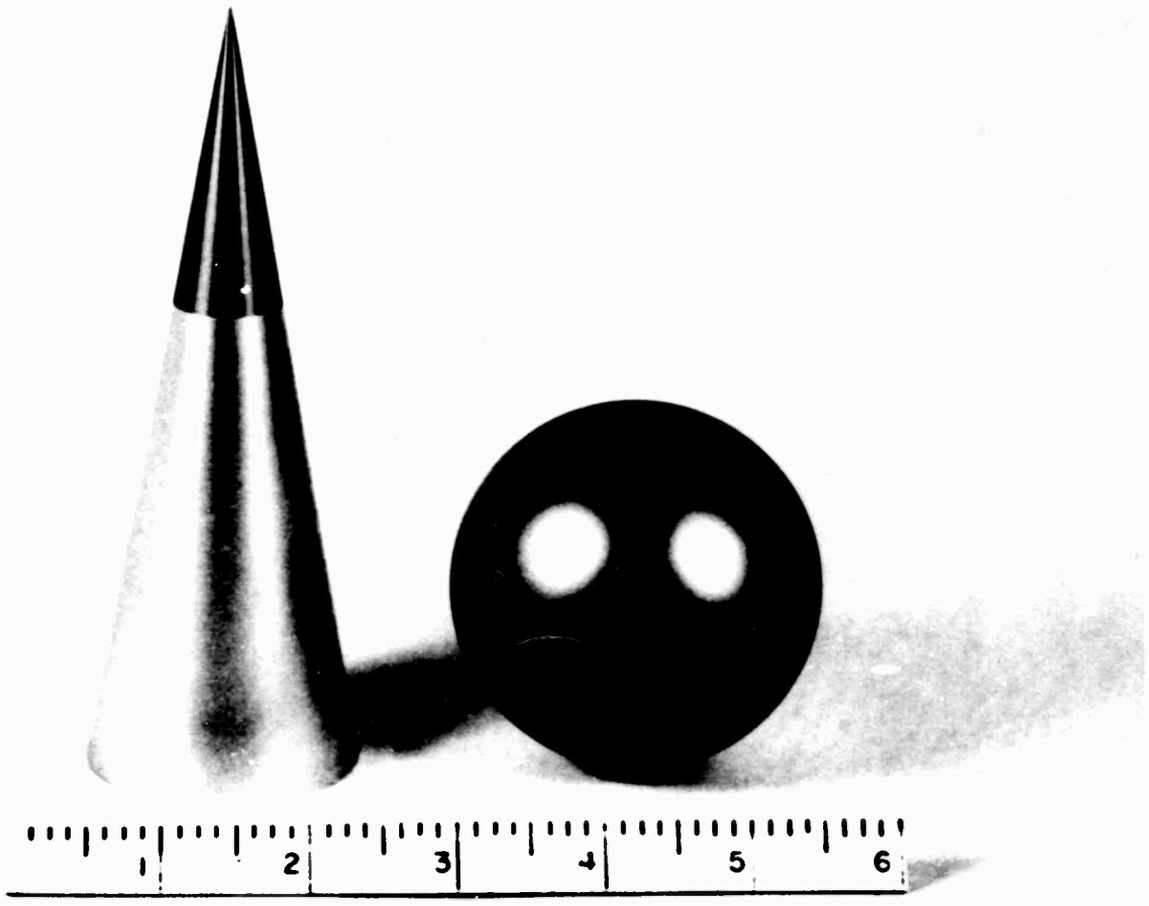

FIGURE 3 - Typical projectiles launched by the four inch gun.

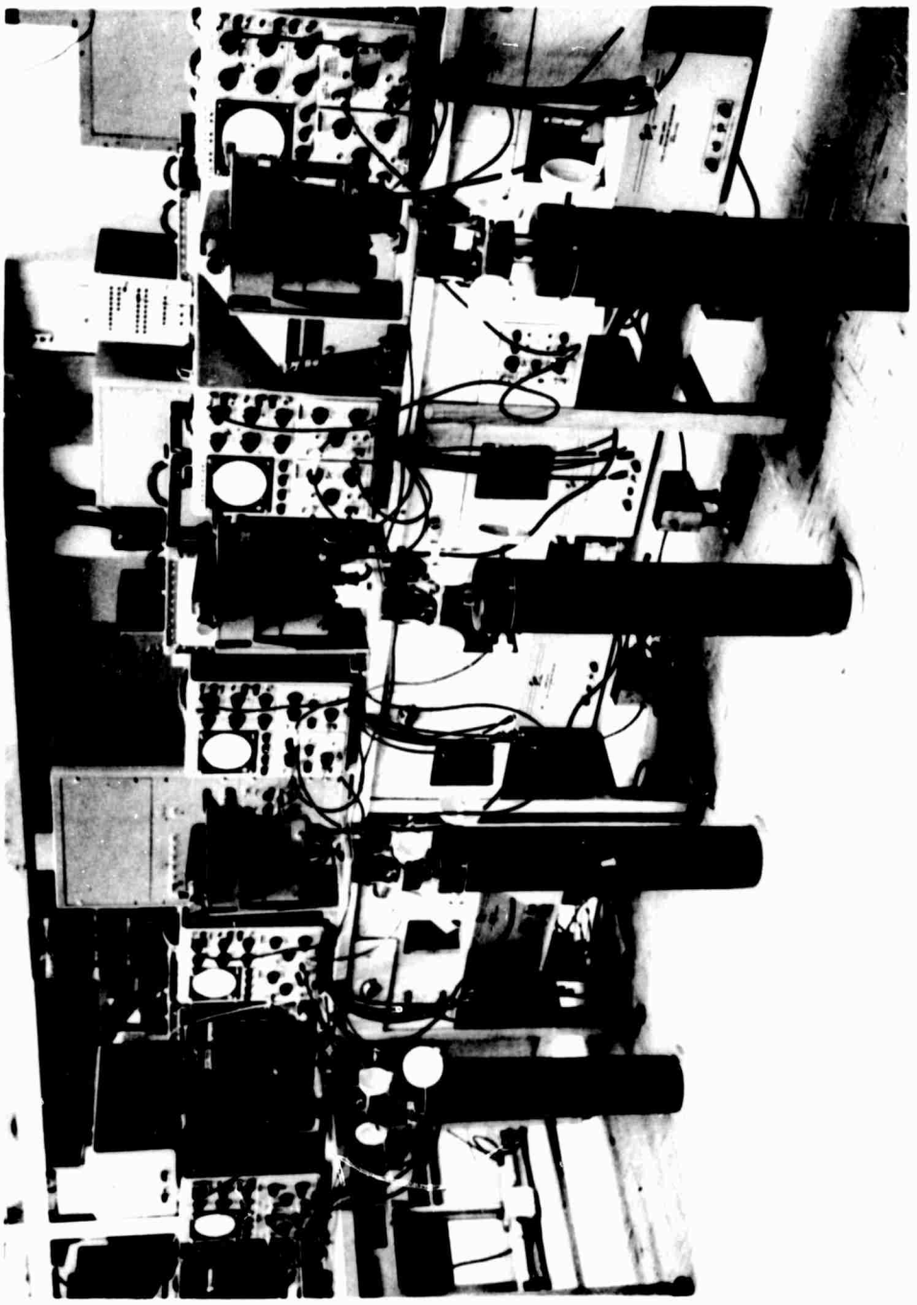

FIGURE 4 - Recording installation of oscilloscopes and Fastax cameras.

FIGURE 5 - Stereo-photographs of three sequences of sparks made behind a one inch diameter aluminum sphere at three axial distances (from left to right X/D = 450, 1000 and 2400 B.D.).
V_∞ = 14.3 kfps, P_∞ = 40 torr.

FIGURE 6 - Stereo-photograph of a sequence of sparks obtained behind a one inch diameter aluminum sphere.
X/D = 600 V_∞ = 14.6 kfps P_∞ = 40 torr.

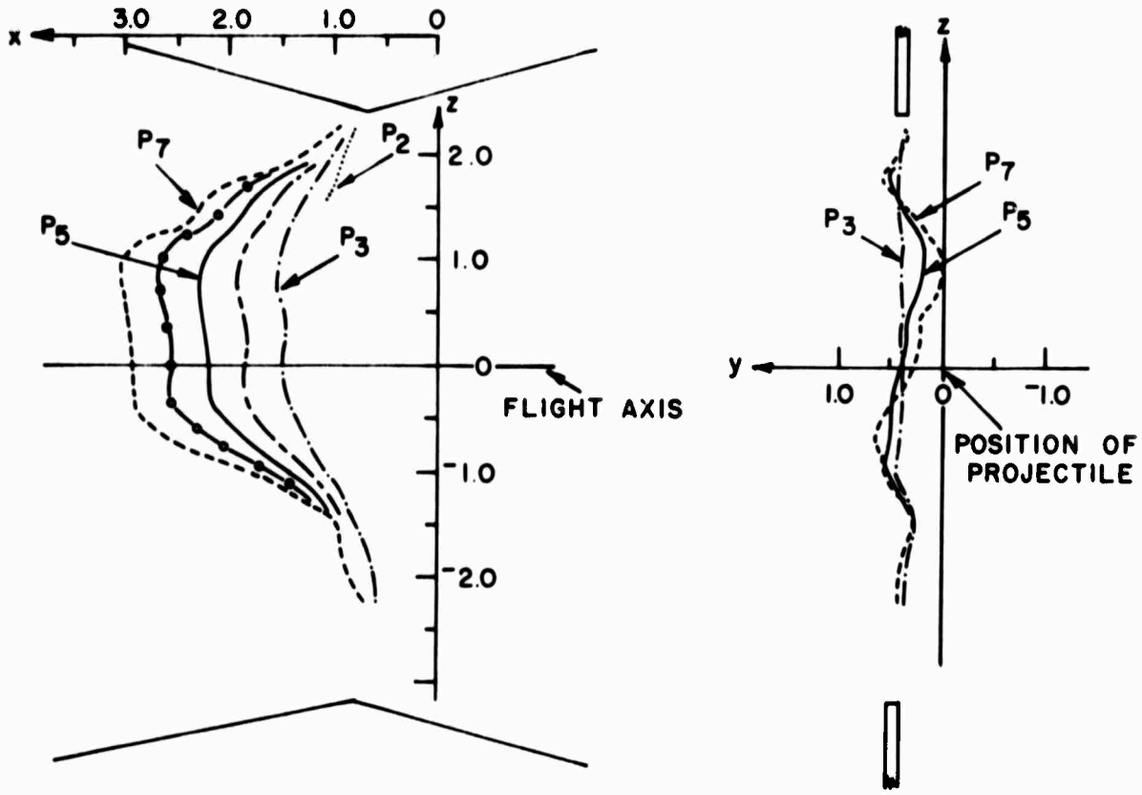

FIGURE 7 - Projections in the XZ (axial) and YZ (lateral) plane of the series of sparks of Figure 6

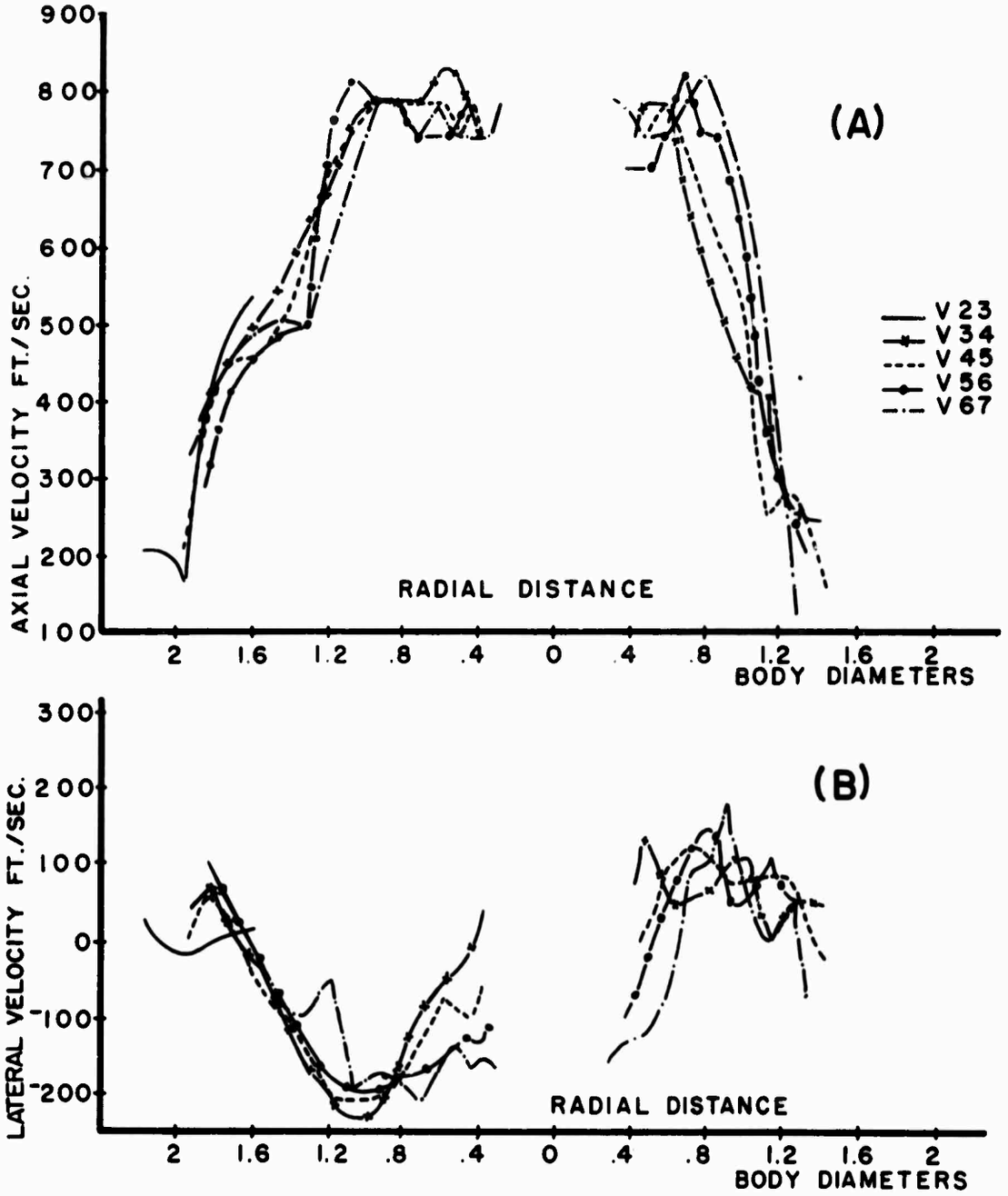

FIGURE 8 - Radial profiles of the axial and lateral wake velocities obtained via the sequence of sparks of Figure 6

FIGURE 9 - Axial array of electrostatic probes.

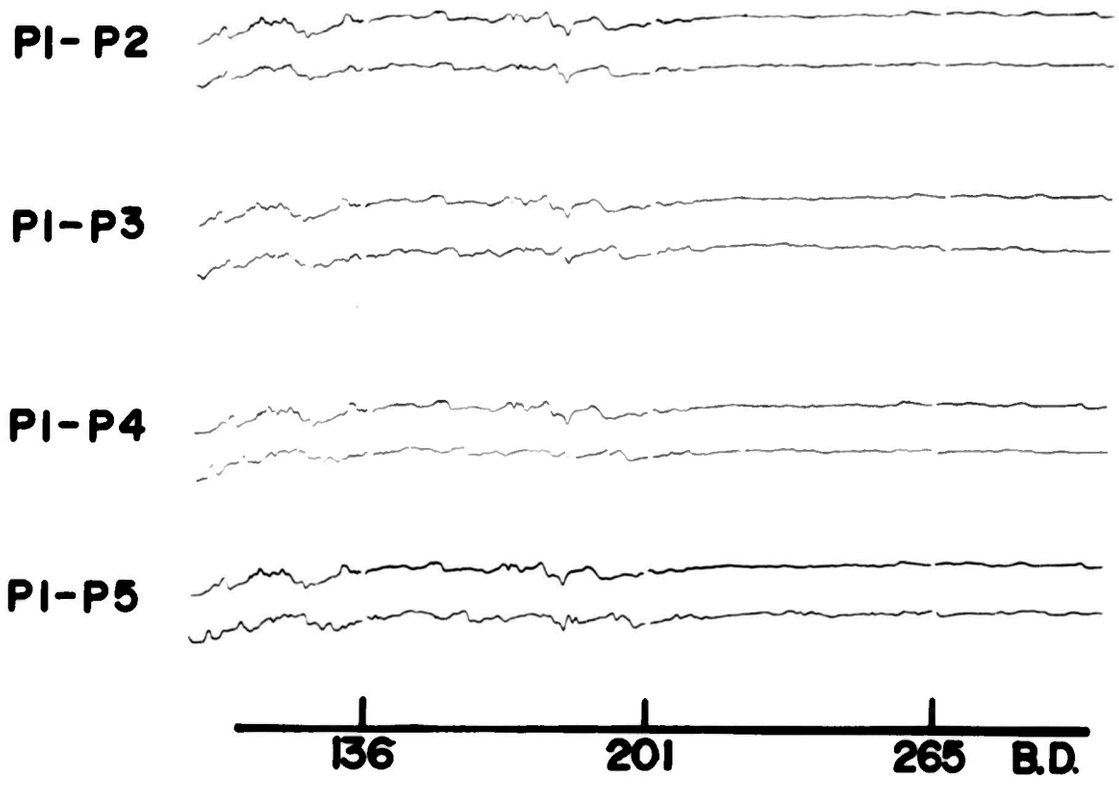

FIGURE 10 - Segments of a set of typical electrostatic probe axial array current signals obtained behind a 2.7 inch Ti sphere V_∞ = 14.5 kfps P_∞ = 9.3 torr R/D = 0.6 B.D.

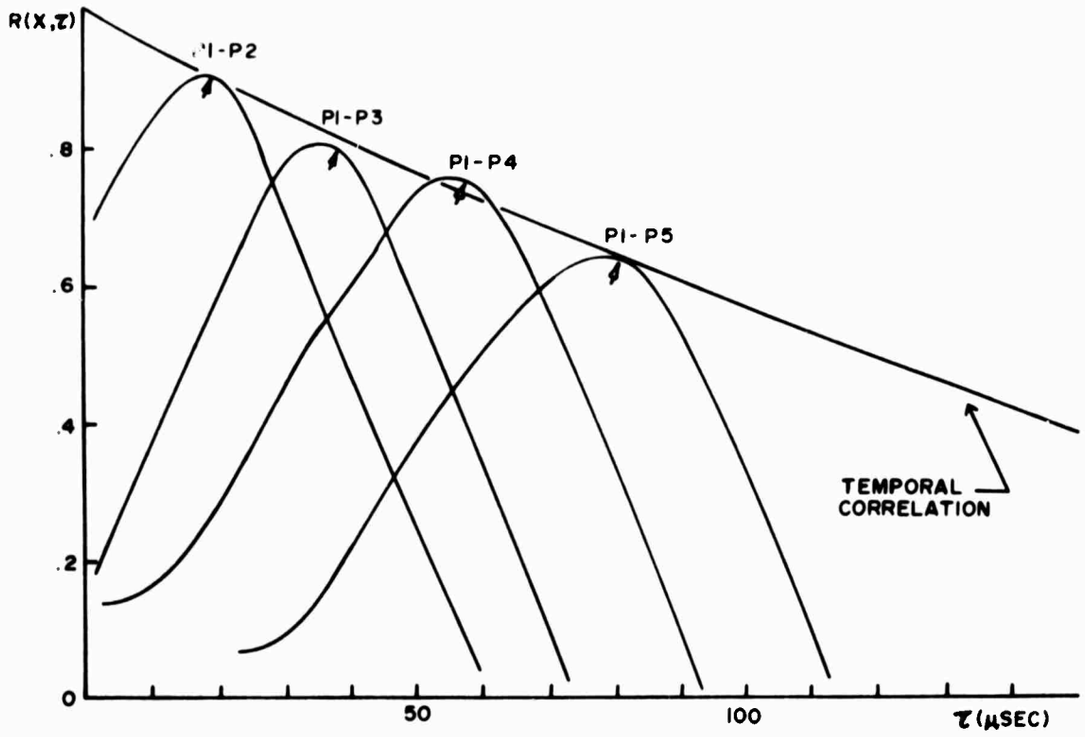

FIGURE 11 - Family of cross correlation $R(x, \tau)$ curves obtained by cross correlating corresponding 0.5 millisecond sections from the pairs of probe current signals shown in Figure 10. The envelope of the curves represents the autocorrelation in the moving frame (temporal correlation).

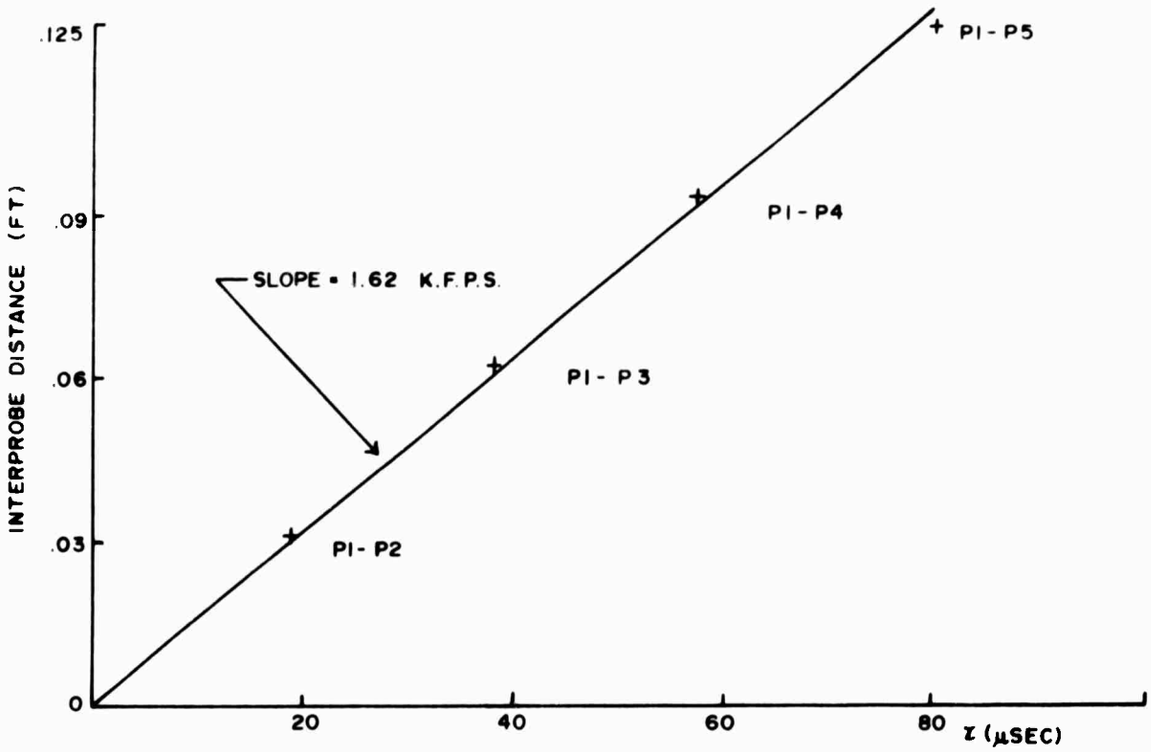

FIGURE 12 - Convection velocity determination using the data shown in Figure 11

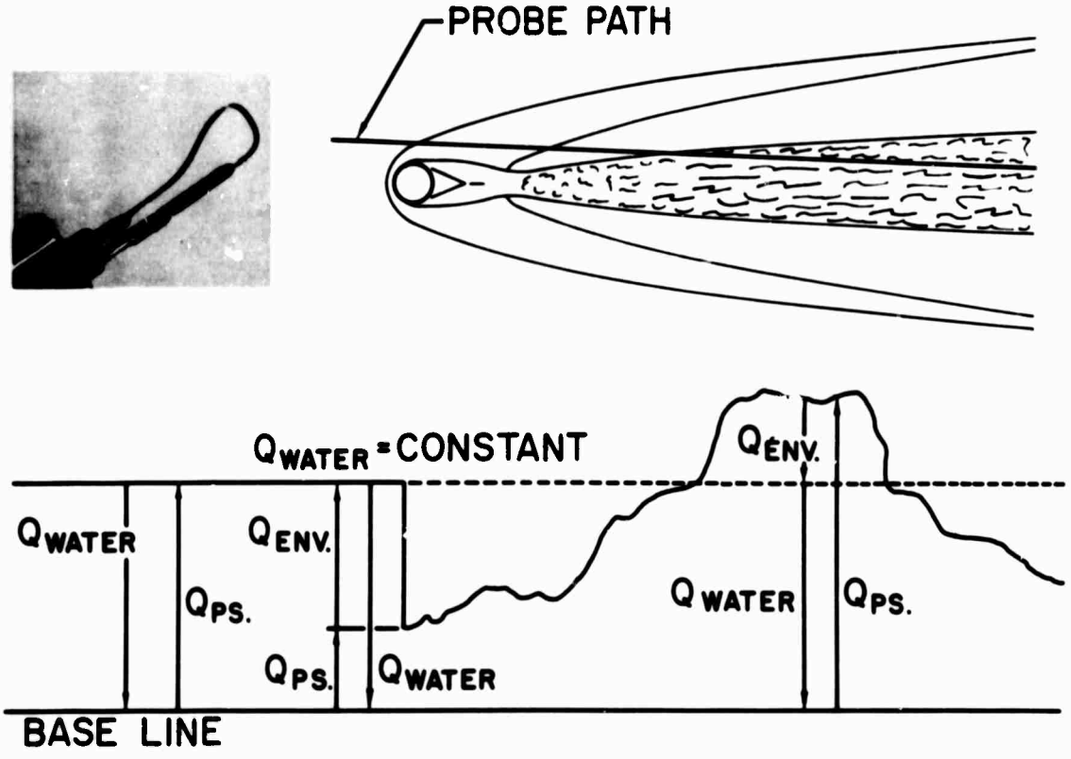

FIGURE 13 - Illustration of typical heat flux power balance situations for the cooled film anemometer. The insert shows the sensor element.

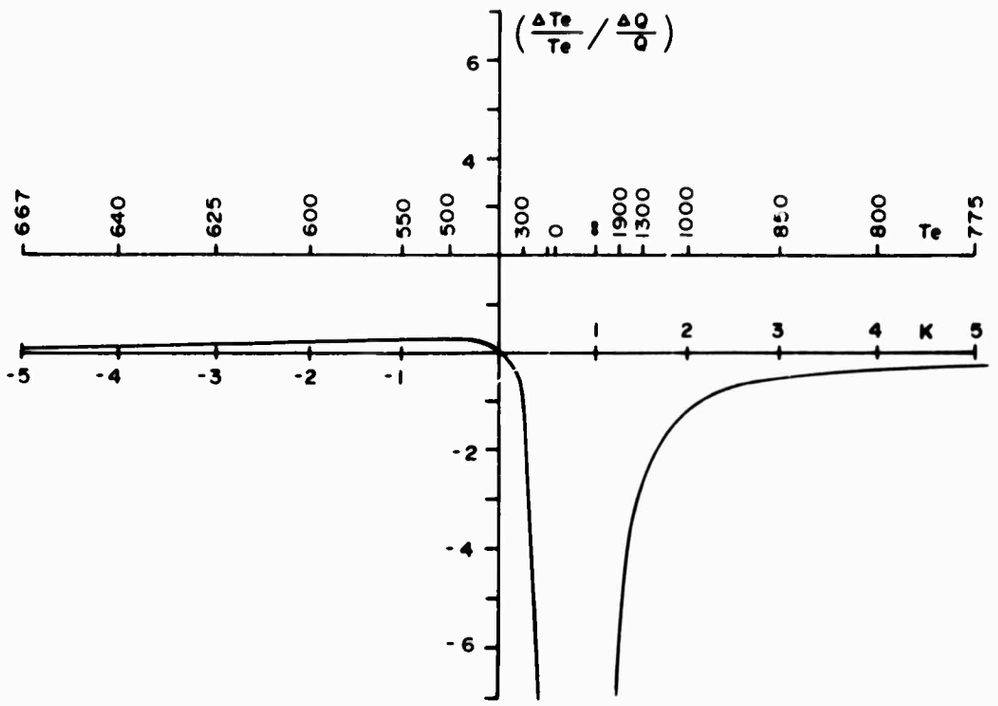

FIGURE 14 - Errors induced in the determination of the flow temperature by fractional errors in the input data for operating temperatures of 400 and 700° Kelvin. (Ellington, Private Communication).

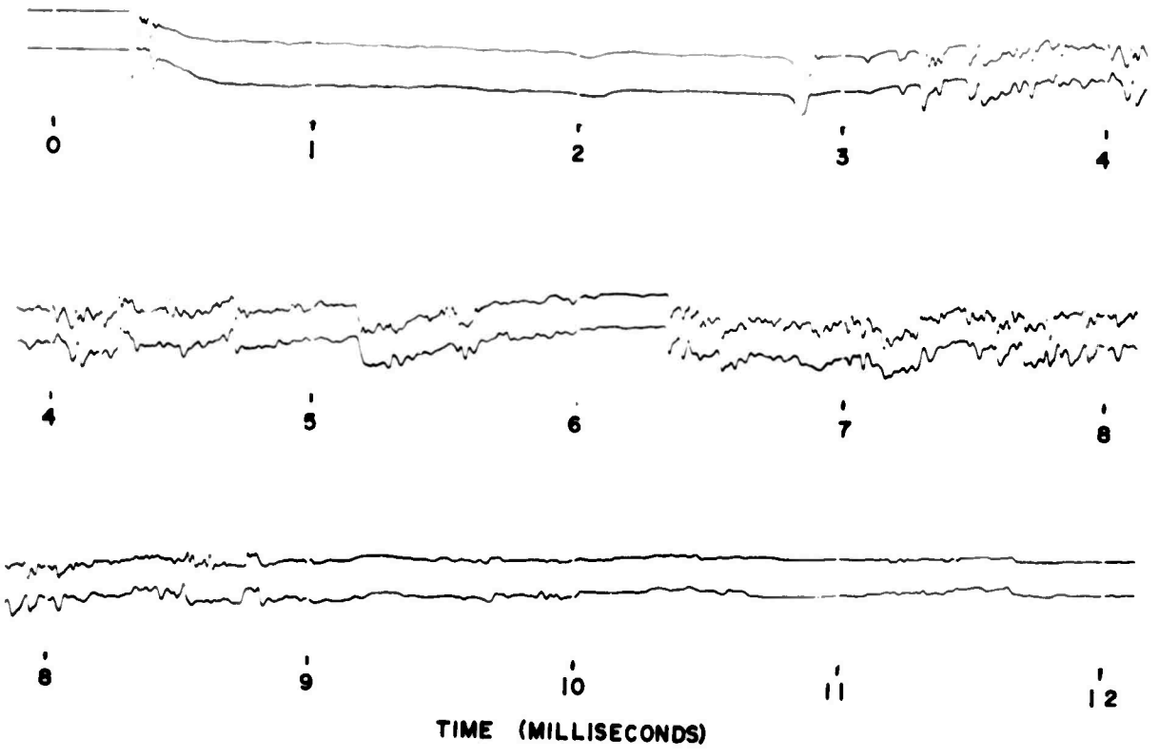

FIGURE 15 - Fluctuating voltage signal from two cooled film anemometers in a 2.7 inch sphere wake with minimum spacing between the sensors. The bow shock occurs about 0.3 millisecond after the zeroth timing mark. The probes traverse the inviscid wake until about the 3rd timing mark, when they encounter the viscous core. The sensor temperatures were 423° and 678° Kelvin.
V_∞ = 14.6 kfps P_∞ = 75.9 torr R/D = 2.2 BD
(Ellington, Private Communication).

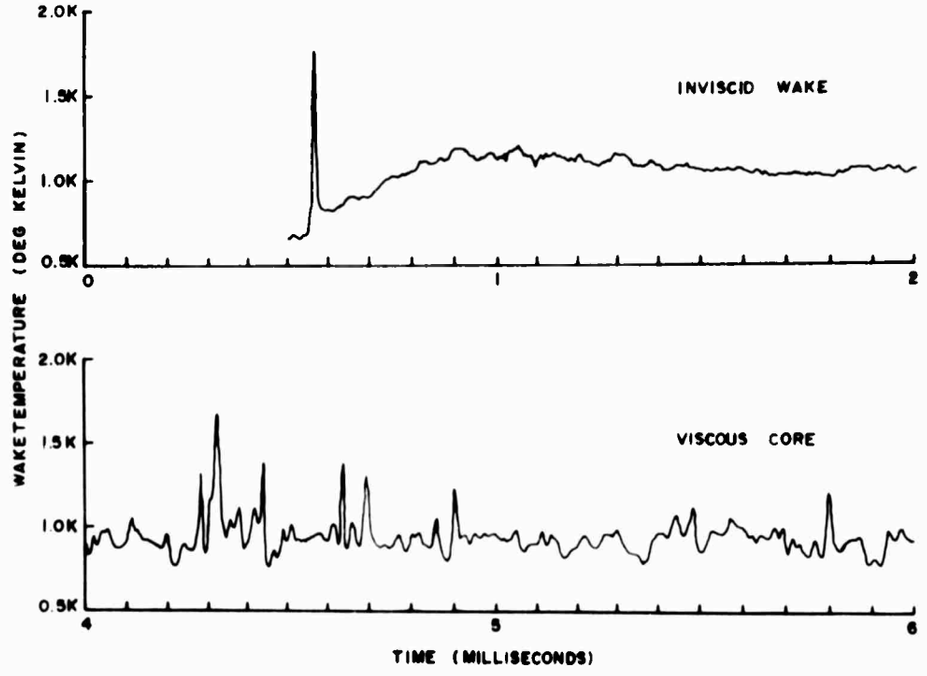

FIGURE 16 - Temperature in the inviscid wake and viscous core obtained from analysis of the signals of Figure 15. (Ellington, Private Communication).

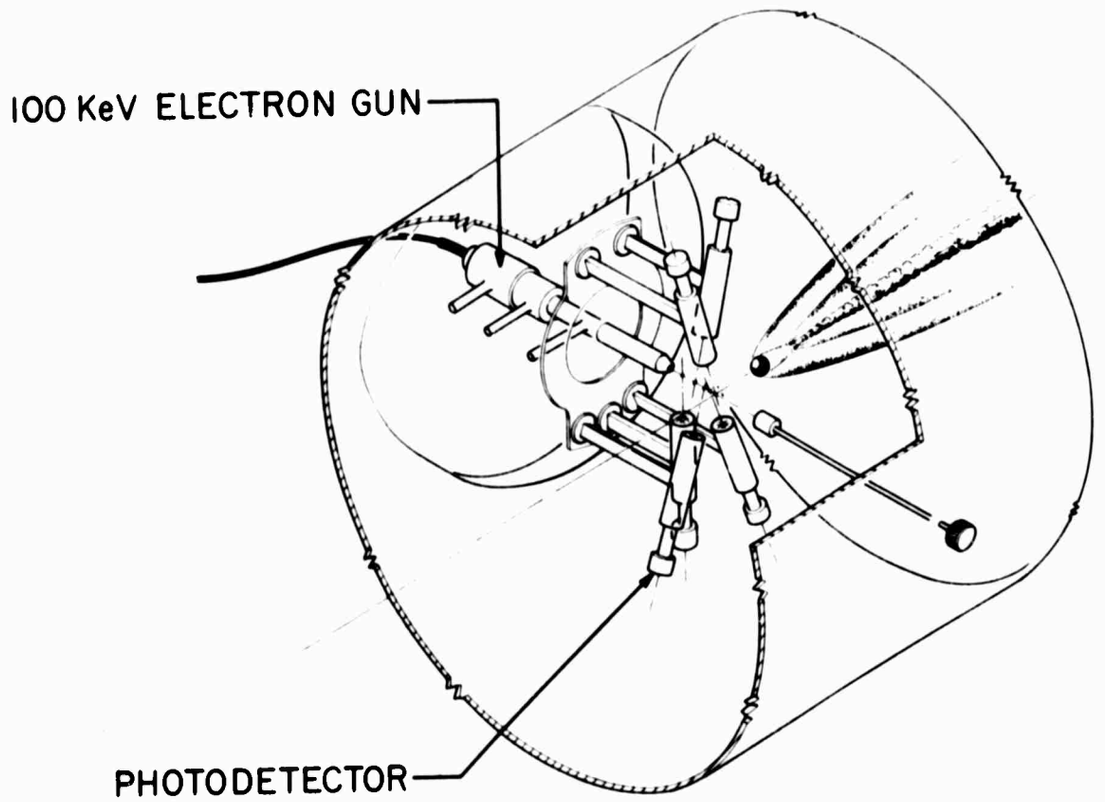

FIGURE 17 - Schematic of Electron Beam equipment on Range 5.

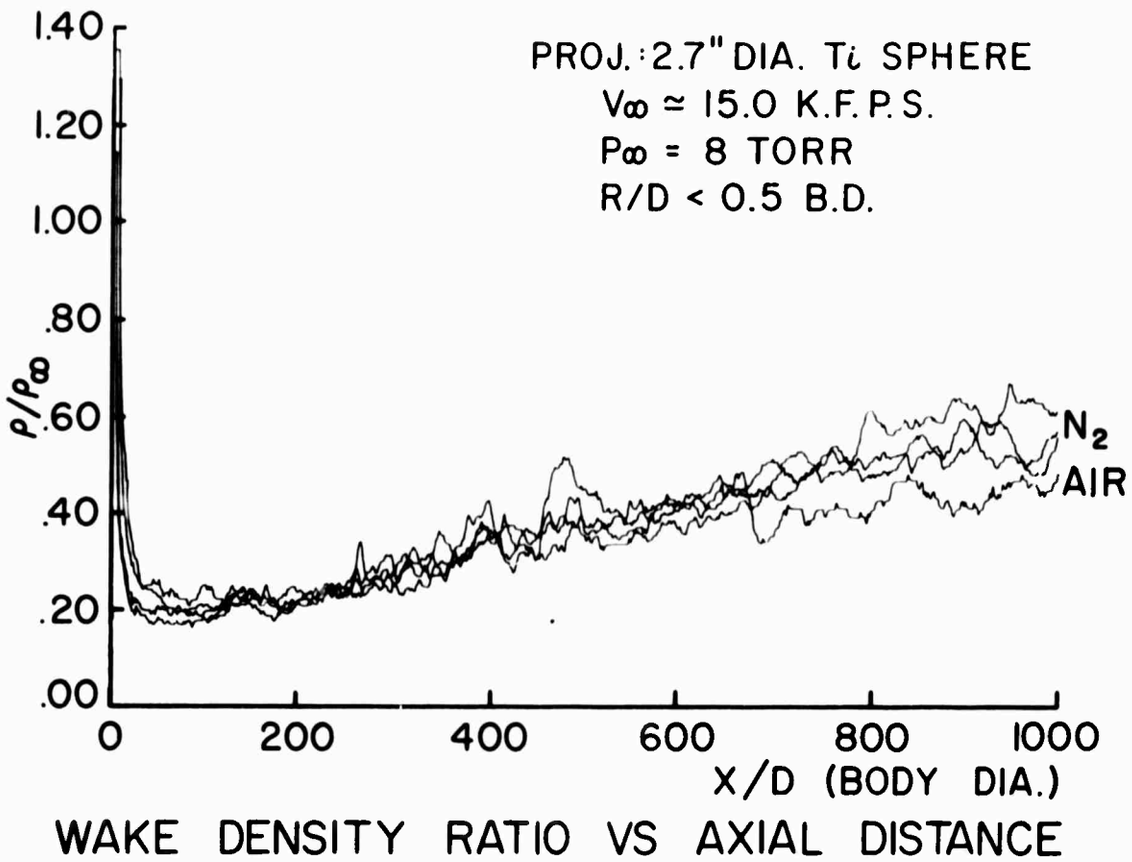

FIGURE 18 - Typical measurements of mass density normalized to free stream density near the wake axis as obtained with the electron beam equipment. Correction for the reduction of attenuation of the beam in the presence of the wake would slightly lower the estimates of normalized wake mass density on the axis.
V_∞ = 15 kfps P_∞ = 8 torr R/D < 0.5 BD

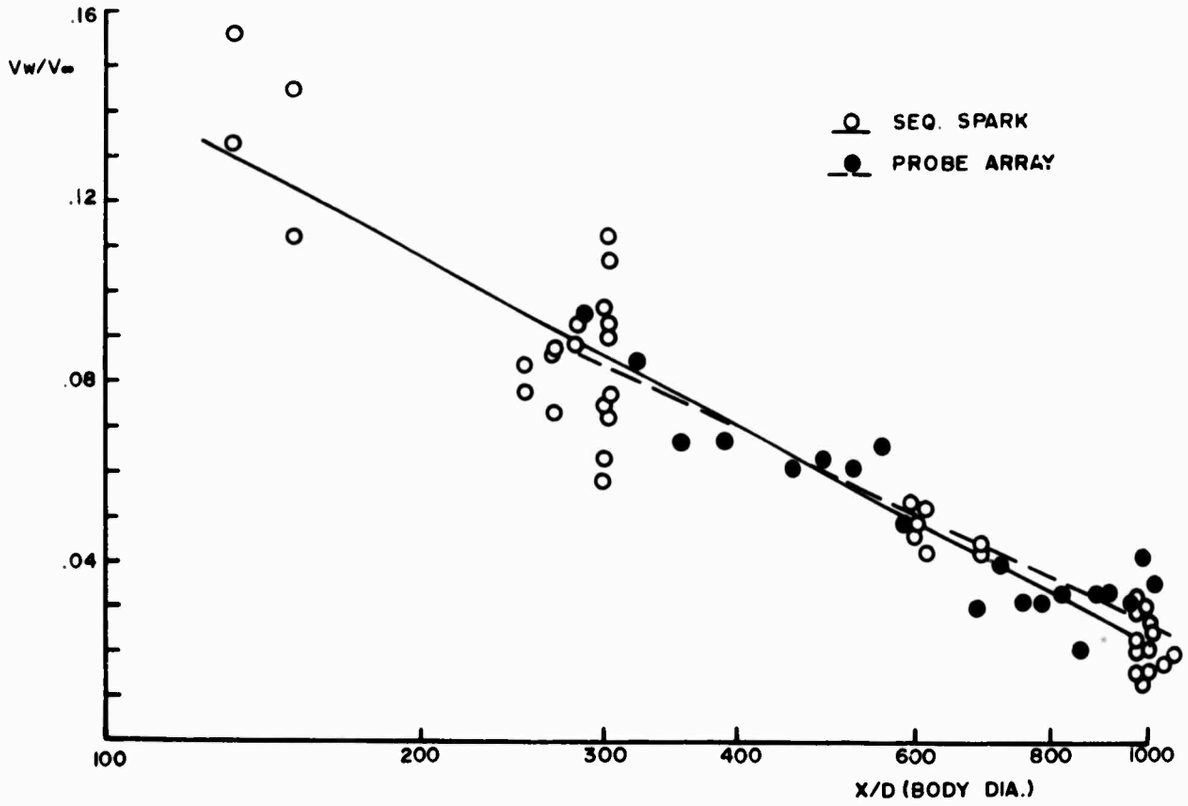

FIGURE 19 - Semilogarithmic rms fits of sequential spark and probe array normalized wake velocity data, compared at R/D = 0.7. The sequential spark data were obtained on 40 rounds at the following conditions: one inch diameter spheres $12 \leq V_\infty \leq 15$ kfps, and $20 \leq P_\infty \leq 76$ torr. The probe array data were obtained on one 2.7 inch diameter sphere firing at 15 kfps and 21 torr.

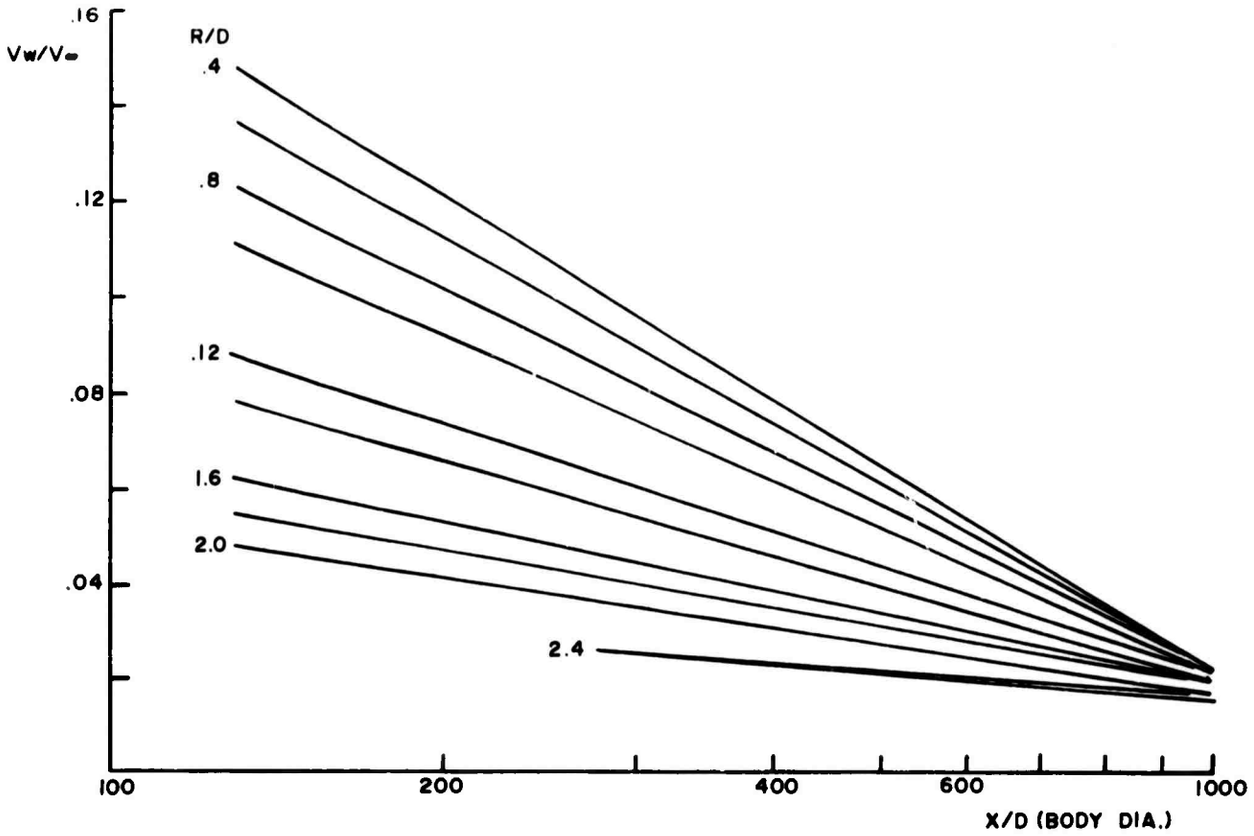

FIGURE 20 - Family of mean axial wake velocity profiles at various radial distances R/D using semilogarithmic rms fits.
One inch diameter spheres
$12 \leq V_\infty \leq 15$ kfps $\qquad 20 \leq P_\infty \leq 76$ torr.

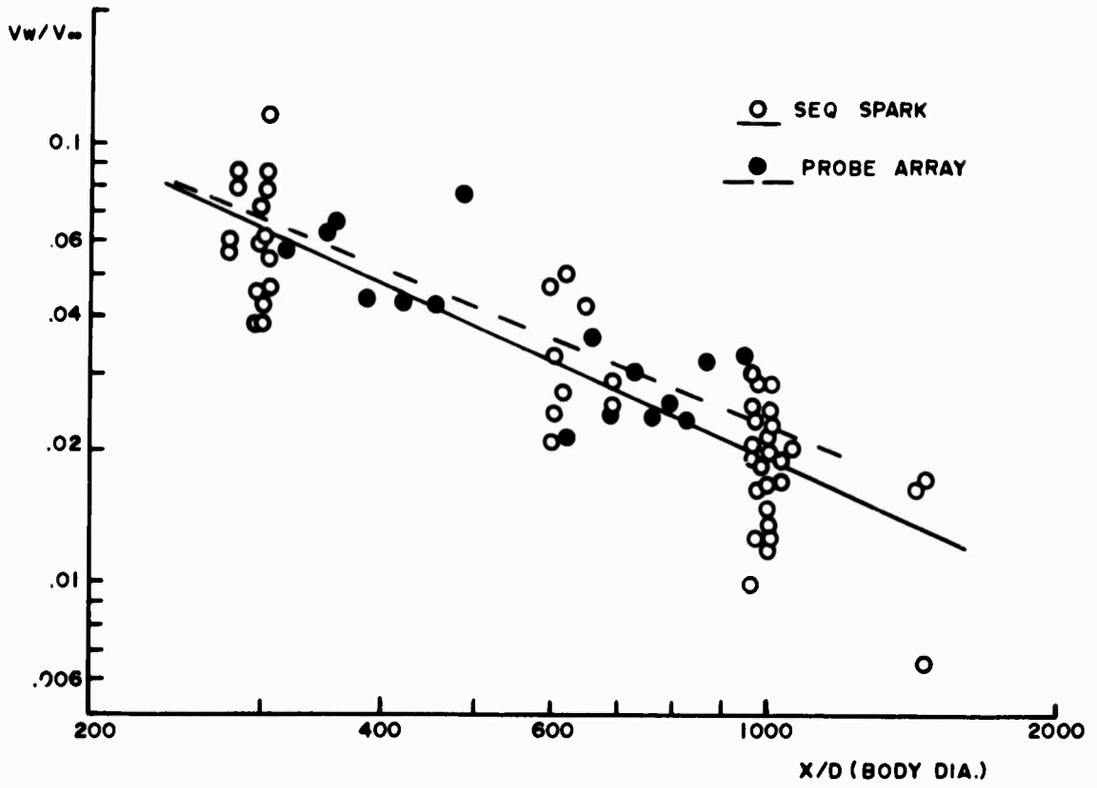

FIGURE 21 - Logarithmic rms fits of sequential spark and probe array normalized wake velocity data at R/D = 1.2 BD. The sequential spark data were obtained on 40 rounds at the following conditions: one inch diameter spheres, $12 \leq V_\infty \leq 15$ kfps, and $20 \leq P_\infty \leq 76$ torr. The probe array data were obtained on a 2.7 inch diameter sphere firing at $V_\infty = 15$ kfps and $P_\infty = 21$ torr.

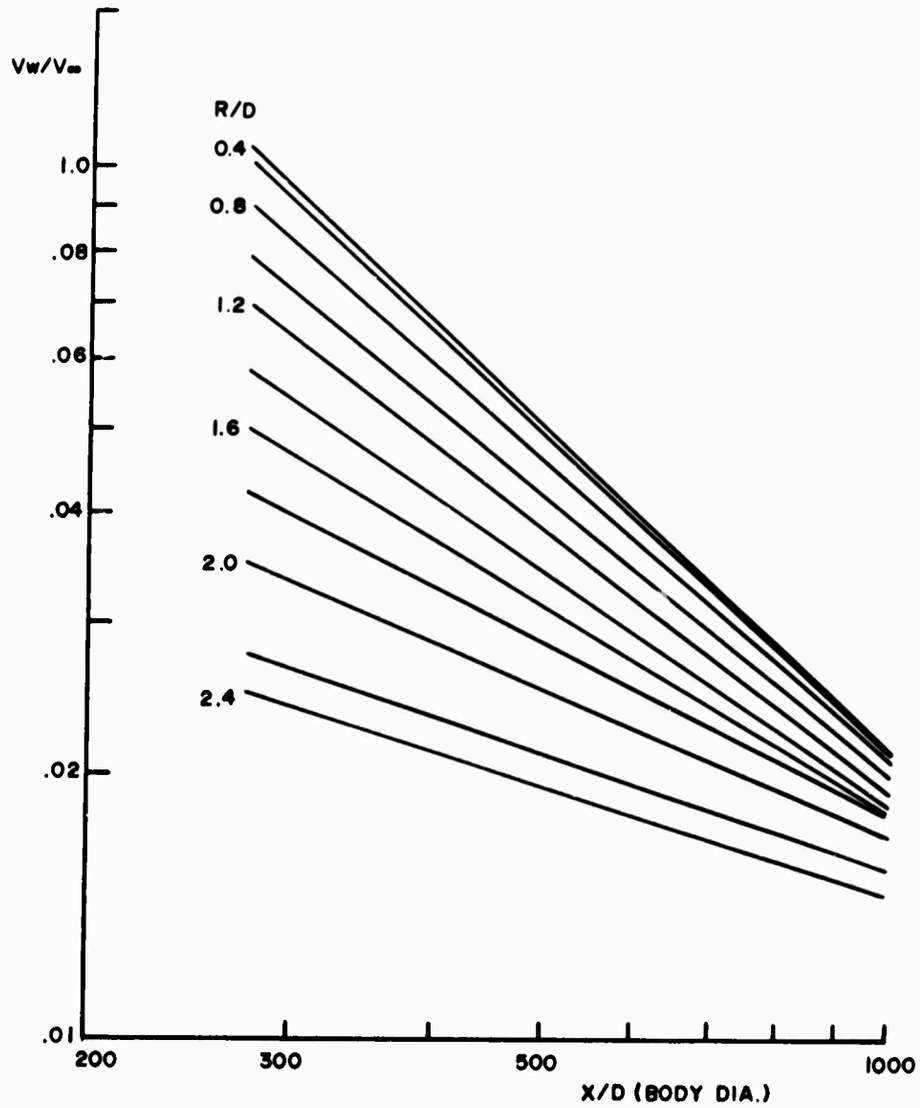

FIGURE 22 - Family of mean axial wake velocity profiles at various radial distances R/D using log rms fits. (Same data as Figure 20 except data points for $X/D < 300$ have been dropped).

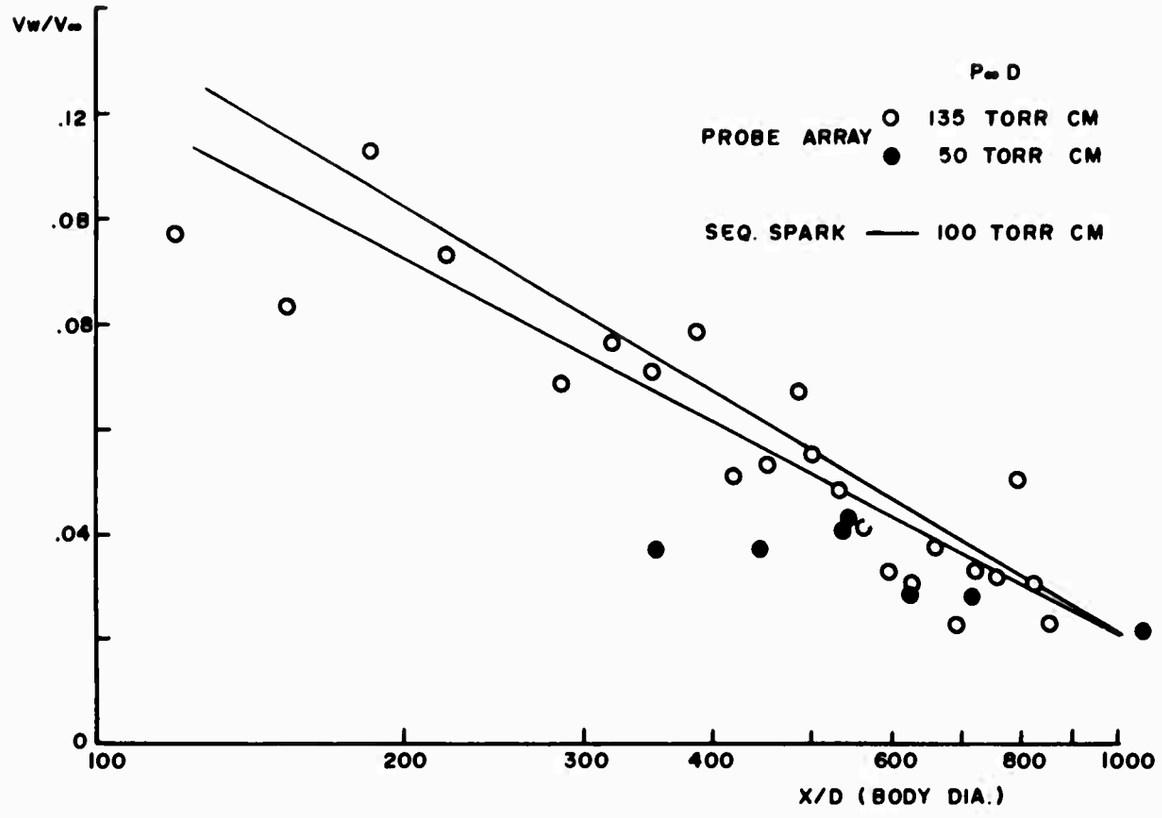

FIGURE 23 - Comparison of electrostatic probe array wake velocity data with the sequential spark data of Figure 20 (R/D = 0.8 and 1.0 BD). The open points were obtained with 2.7 inch diameter spheres at 20 torr ($P_\infty D$ = 135 torr-cm) while the solid points were obtained with one inch diameter spheres at the same pressure ($P_\infty D$ = 50 torr-cm). Velocities were between 14 and 15.5 kfps.

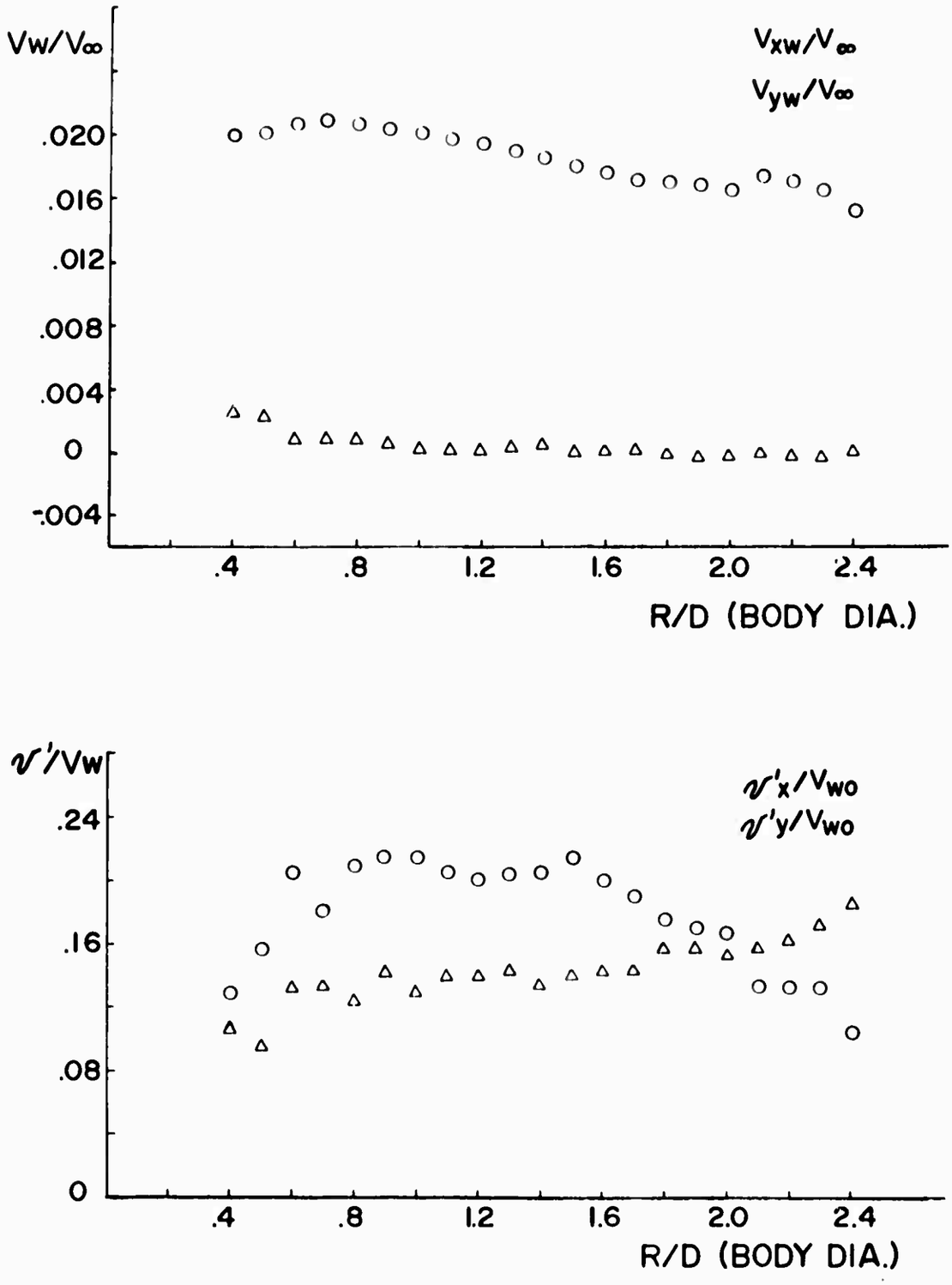

FIGURE 24 - Mean wake velocity profile at X/D = 1000 deduced from 11 sphere firings. V_∞ = 15,000 fps P_∞ = 20 torr. The rms velocity deviation of the data obtained from the average over the individual rounds is also given.

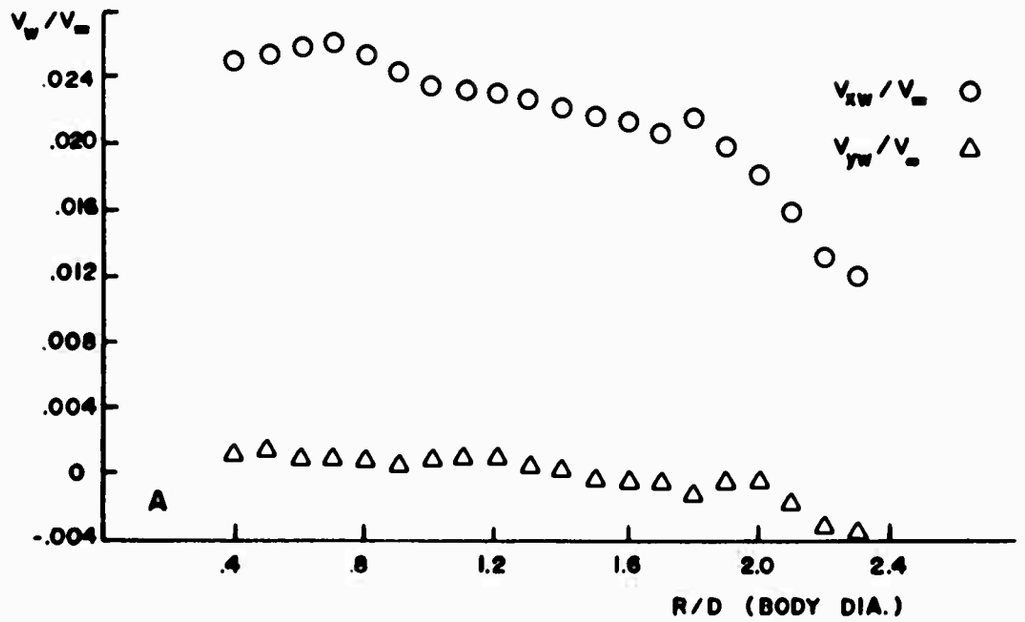

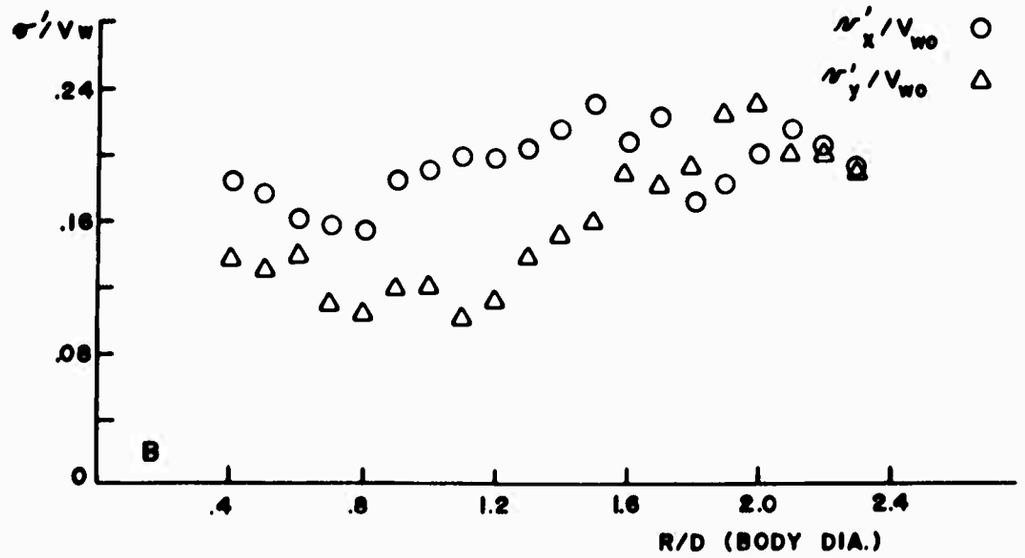

FIGURE 25 - Mean wake velocity profiles at X/D = 1000 deduced from 6 sphere firings. V_∞ = 15,000 fps P_∞ = 76 torr. The rms velocity deviation of the data obtained from the average over the individual rounds is also given.

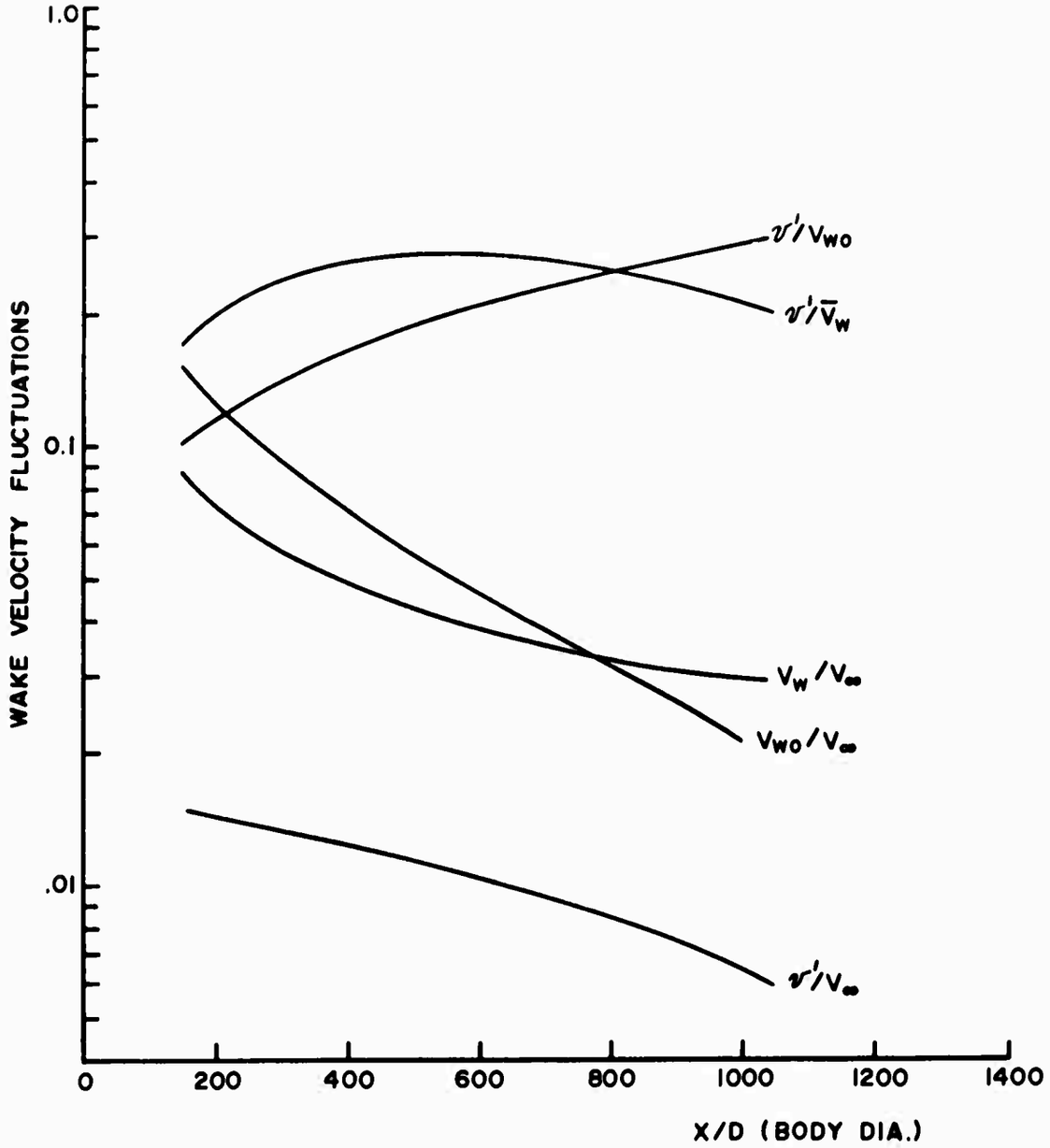

FIGURE 26 - Wake velocity fluctuations inferred from the electrostatic probe array data, averaged over radial distances from 1.0 to 1.5 body diameters. The fluctuation data have been normalized to the mean wake velocity $\bar{V}w$ deduced by the probes for $1.0 \leq R/D \leq 1.5$ and also by the axial wake velocity Vwo measured by the sequential spark experiment.

FIGURE 27 - Sequence of successive schlieren photographs of a hot filament in a hypersonic turbulent wake. Film speed is 18,000 frames/second (60 μseconds per frame). One inch diameter sphere, V_∞ = 10 kfps, P_∞ = 40 torr, X/D = 1200 B.D.

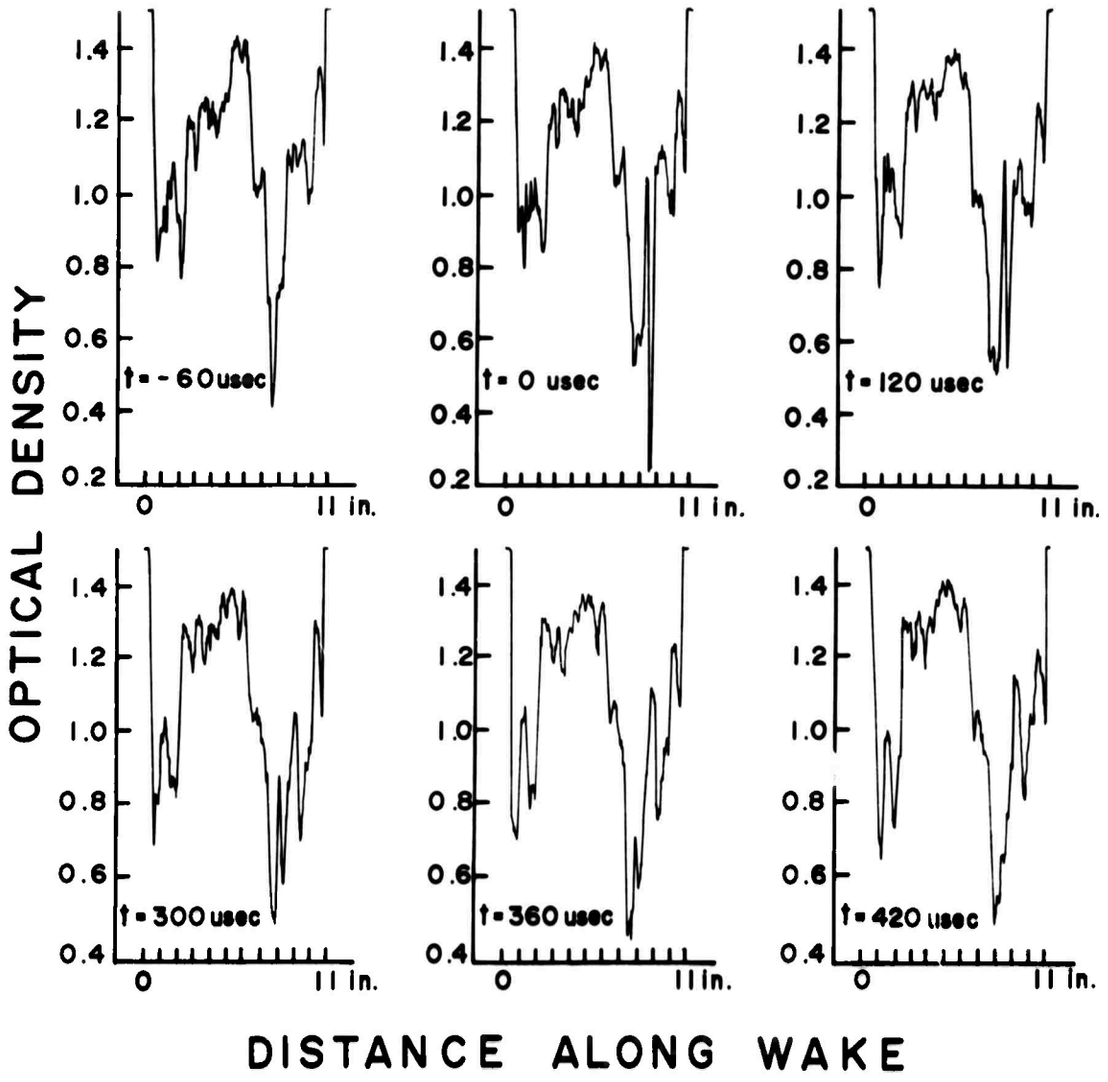

FIGURE 28 - Microdensitometer traces obtained by reading schlieren photographs of Figure 27. Slit width was equivalent to 2 body diameters long by .02 body diameters wide.

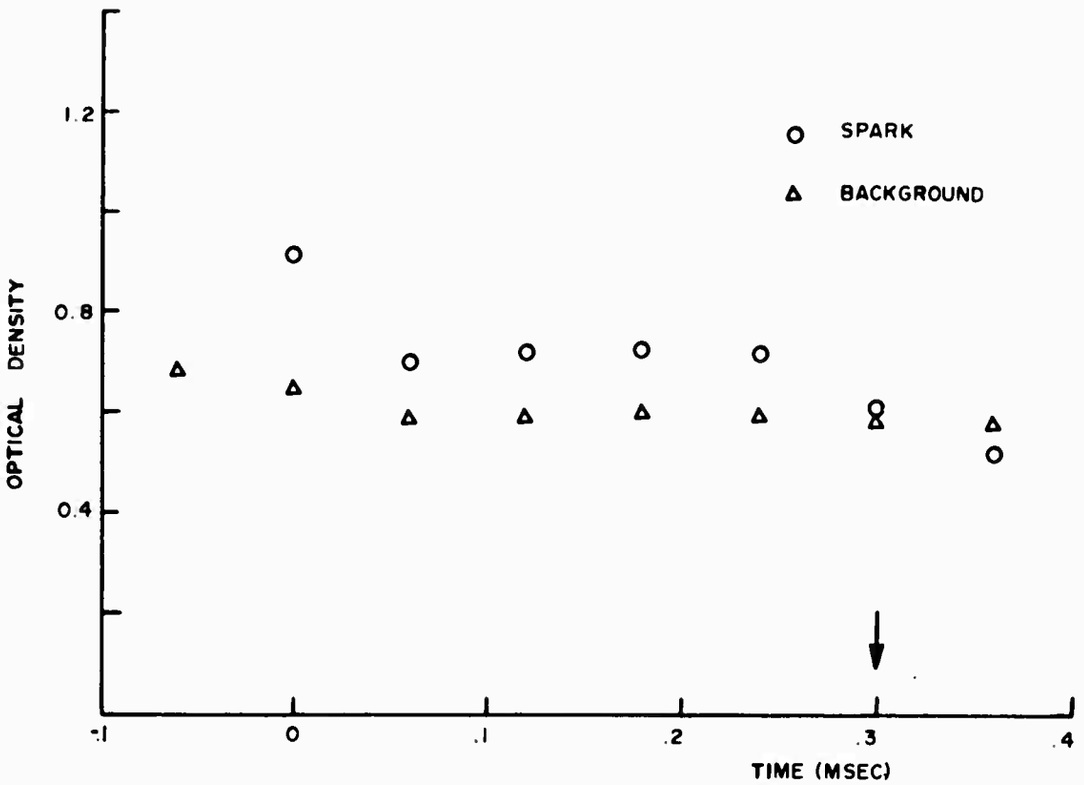

FIGURE 29 - Comparison of average peak amplitude of spark with average background fluctuations from microdensitometer traces.

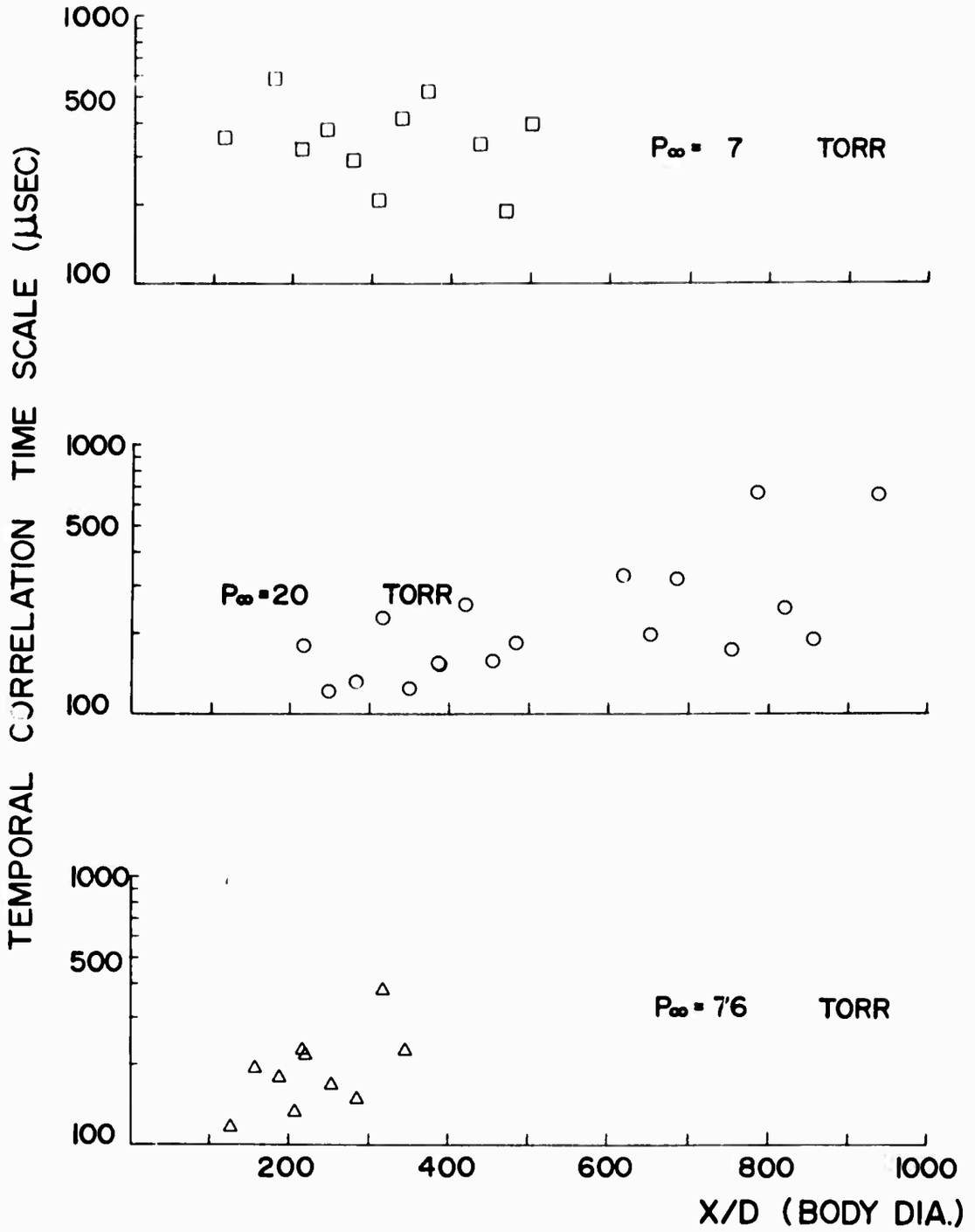

FIGURE 30 - Moving frame autocorrelation time scales as a function of axial distance obtained with the probe array at various pressures.
2.7 inch diameter spheres $14 \leq V_\infty \leq 15$ kfps.